DEVELOPMENT OF HYDROCARBON-CO_2 BLENDS AS WORKING FLUIDS FOR VAPOR POWER CYCLES

A Thesis

by

MOHAMMAD KAZIM

Submitted to the Graduate and Professional School of Texas
A&M University
in partial fulfillment of the requirements for the degree of

MASTER OF SCIENCE

Chair of Committee,	Reza Sadr
Co-Chair of Committee,	Michael Pate
Committee Members,	Pavel Tsvetkov
Head of Department,	Guillermo Aguilar

December 2021

Major Subject: Mechanical Engineering

ABSTRACT

The study examines the performance of zeotropic mixtures consisting of different hydrocarbons with carbon dioxide as working fluids for a supercritical organic Rankine cycle. Four hydrocarbons, i.e., dimethyl ether, R1234yf, diethyl ether, and isobutane, are considered in this study based on their flammability and environmental characteristics such as global warming potential, ozone depletion potential, and toxicity. The zeotropic mixtures are developed using the National Institute of Standards and Technology database, REFPROP 9.1, on a molar concentration basis that varies from 0.2 to 0.8 (20% to 80% hydrocarbon). The performance indicators such as cycle efficiency, volumetric power coefficient, exergy destruction, etc., are assessed for different cycle operating pressures and heat source inlet temperatures varying from 400 K to 500 K. After detailed analysis, the dimethyl ether was the best possible working fluid from all the pure hydrocarbons considered in this study, whereas the zeotropic mixture of dimethyl ether and carbon dioxide was the optimal working fluid from all the zeotropic blends considered. Finally, the performance of the optimal zeotropic mixture was assessed for a system located in Houston, TX using the lowest and highest annual temperature of Houston (i.e., 278 K and 308 K). The results showed that the zeotropic mixture of dimethyl ether and carbon dioxide performs better at lower heat sink temperature (i.e., during winter conditions) with a maximum cycle efficiency of 17.7% and exergy efficiency of 41.0% at a reduced pressure of 2.12 (13,827 kPa) and a fractional molar concentration of 0.8 (80% hydrocarbon).

ACKNOWLEDGEMENTS

I am thankful to Texas A&M University for providing access to the necessary resources required to complete this research work. I am also grateful for the guidance from my Advisor Dr. Reza Sadr and Co-Advisor, Dr. Michael Pate, for their efforts behind this work.

I would also like to thank my friend and fellow researcher, Mr. Debranjan Das, who has supported me and co-authored my publications. Thanks to my friends and colleagues and the department faculty and staff for making my time at Texas A&M University a great experience.

Finally, thanks to my mother and father for their encouragement and love.

CONTRIBUTORS AND FUNDING SOURCES

Contributors

This work was supervised by a thesis committee consisting of Associate Professor Reza Sadr [Advisor] and Professor Michael Pate [Co-Advisor] of J. Mike Walker ’66 Department of Mechanical Engineering and Professor Pavel Tsvetkov of the Department of Nuclear Engineering.

The analyses presented in this study were conducted in part by Mr. Debranjan Das, a graduate student in the J. Mike Walker ’66 Department of Mechanical Engineering was also the first author of the journal article on which the preliminary study is based. The article was published in June 2021.

All other work conducted for the thesis was completed by the student independently.

Funding Sources

The graduate study was supported by Byron Anderson ‘54 fellowship from the Department of Mechanical Engineering, Texas A&M University, amounting to $1000 with a non-resident tuition waiver for the 2020-2021 academic year and a $3000 grant from the State of Texas. This research did not receive direct financial support or grants from funding agencies for completion.

NOMENCLATURE

N	Annual Operating Hours
CRF	Capital Recovery Factor
CO_2	Carbon Dioxide
CFC	Chlorofluorocarbon
COP	Coefficient of Performance
c	Cost per unit Exergy ($/GJ)
$\dot{C}$	Cost Rate ($/h)
DEE	Diethyl Ether
DME	Dimethyl Ether
EES	Engineering Equation Solver
$\dot{XD}$	Exergy Destruction Rate (kW)
$\dot{EX}i$	Exergy Rate at State Point I (kW)
GWP	Global Warming Potential
$\dot{Q}$	Heat Rate (kW)
HC	Hydrocarbon
HFC	Hydrofluorocarbon
i_r	Interest Rate (%)
LMTD	Logarithmic Mean Temperature Difference
$\dot{m}$	Mass Flow Rate (kg/s)
NIST	National Institute of Standards and Technology

ORC	Organic Rankine Cycle
U	Overall Heat Transfer Coefficient
$\dot{W}$	Power (kW)
P	Pressure (kPa)
PEC	Purchase Equipment Cost
RC	Rankine Cycle
h	Specific Enthalpy (kJ/kg)
s	Specific Entropy (kJ/kg-K)
SORC	Supercritical Organic Rankine Cycle
SRC	Supercritical Rankine Cycle
n	System Lifetime
T	Temperature (K)
δT_1	Temperature difference in the evaporator
δT_2	Temperature difference in the condenser
$Z_k^{\cdot}$	Total Cost Rate for the kth component
VCRC	Vapor Compression Refrigeration Cycle
VPC	Volumetric Power Coefficient (MJ/m^3)
WF	Working Fluid

Greek Alphabets

η	Energy Efficiency (%)
σ	Fractional Molar Concentration

λ	Non-dimensional Exergy Destruction
ϕ	Normalized Reduced Pressure
θ	Reduced Pressure

Subscripts

cs	Cold Source
hs	Hot Source
c	Condenser
e	Evaporator
p	Pump
t	Turbine
in	Inlet
out	Outlet
s	Second Law

TABLE OF CONTENTS

Page

LIST OF FIGURES

Page

LIST OF TABLES

Page

1. INTRODUCTION

A substantial amount of energy generated in the world is lost as waste heat. According to the U.S. Department of Energy, an estimate of 20-50% of industrial energy input is lost as waste heat in the form of hot exhaust gases and heat lost from equipment, etc. [1]. The manufacturing sector in the U.S. alone has annual process heating energy losses of 747.6 TWh, of which approximately 15.4% (113.6 TWh/year) can be recovered from high-temperature exhaust gases [2], [3]. Recovery of this waste heat may improve the system's energy efficiency, reduce the environmental impact, generate cost-saving, and improve productivity. A significant problem for the recovery of this waste heat is the “low temperature” of the wasted heat that makes recovery inefficient. Several technologies and methods are available for recovering this waste heat, including economizers, waste heat boilers, air preheaters, plate heat exchangers, Kalina cycle, etc. One of the most popular and effective methods of recovering waste heat from low-temperature sources is an organic Rankine cycle (ORC). Using an ORC as a waste heat recovery technology is an economically valuable solution that offers higher performance, flexibility, and lower maintenance and capital costs compared to other available technologies [4].

1.1. Background

Organic Rankine cycles (ORC) use organic working fluids (hydrocarbons etc.) instead of water and steam to generate power from low-grade heat sources. The use of organic fluids enables the cycle to operate at low temperatures. According to the U.S. Department of Energy, low-grade heat or low-temperature heat sources are temperature

sources below 230°C (500 K) [5]. Some primary sources for low-grade heat include Geothermal, Solar, Biomass, Internal Combustion Engines, and Industrial Waste Heat [6][7][8], and ORC technology has been demonstrated as a standard and essential technology to recover this low-grade waste heat [9].

A schematic of the cycle shown in Figure 1 reveals that the ORC has four essential components like the Rankine cycle, including the evaporator, turbine, condenser, and pump. The organic working fluid (WF) leaves the condenser in a saturated-liquid state and enters the pump, increasing its pressure. The WF, now in a compressed liquid state, is fed to the evaporator, where a low-temperature heat source transfers its heat energy to the WF. The WF in a superheated-vapor state then enters the turbine where it undergoes expansion, i.e., the heat is converted into mechanical energy and then into electrical power using a generator. The WF leaves the turbine in a saturated-vapor state and enters the condenser. Inside the condenser, the WF rejects its heat to the heat sink (e.g., cooling water) and converts it into a saturated-liquid state, which is then fed back to the pump.

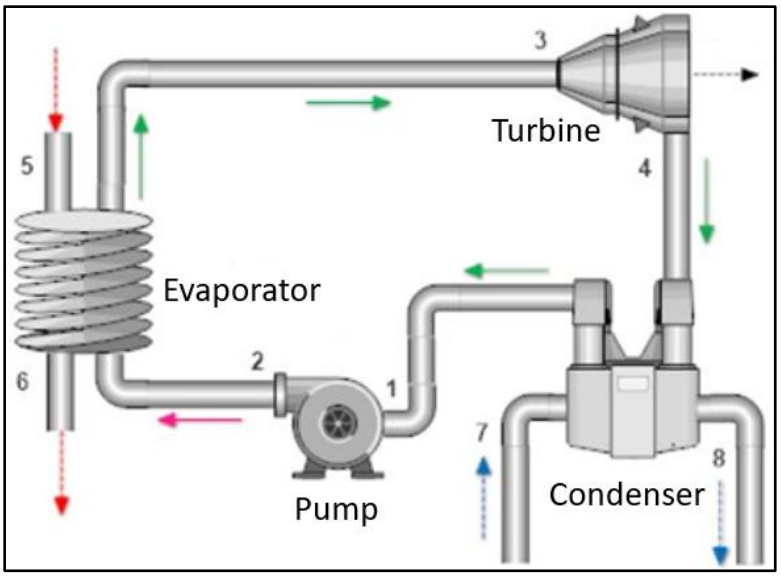

Figure 1. Schematic of the organic Rankine cycle [10]

In a Rankine cycle (RC), during the heat exchange process in the evaporator and condenser, there are temperature differences between the fluids exchanging heat energy, generating irreversibilities (exergy losses) in the cycle components. One method of reducing this exergy loss is by operating the cycle at the supercritical condition [11]. RCs, when operated at supercritical conditions, are commonly referred to as supercritical Rankine cycles (SRC). The WF in a supercritical cycle is heated directly from the saturated-liquid state into the supercritical state, which provides a favorable match of temperature profiles in the evaporator, thus minimizing exergy losses. As shown in Figure 2, which is a T-s diagram comparison for subcritical and supercritical Rankine cycles operating with a pure WF.

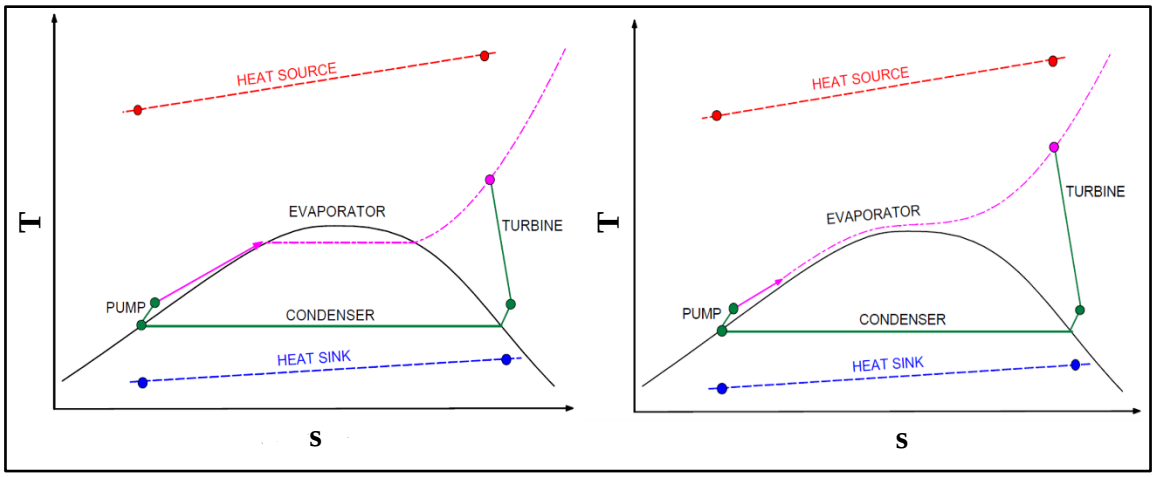

Figure 2. Temperature-Entropy (T-s) diagram for the subcritical Rankine cycle (Left) and supercritical Rankine cycle (Right)

Although an SRC using a pure WF provides a suitable temperature match in the evaporator, the condensation process is still isothermal. One solution to improve the overall efficiency of the RC is to use Zeotropic Mixtures as the WF in a SRC instead of pure fluids, which results in much lower exergy destruction due to a better temperature match in the evaporator and condenser [12]. According to Yelishala et al. [13], the performance of an SRC using zeotropic mixtures can be improved by temperature glide matching in the heat exchangers (evaporator and condenser). For a given composition of the zeotropic mixture, the temperature glide is defined by Yelishala et al. [14] as the temperature difference between the boiling and dew points during the phase change. The temperature glide for pure refrigerants is zero, whereas it has a maximum value for a specified composition of the zeotropic mixture. Figure 3 shows the T-s diagram for a supercritical Rankine cycle using the zeotropic mixture as the WF. Since most of the waste

heat is at low temperatures, organic WFs are often used for the zeotropic mixture in the so-called supercritical organic Rankine cycle (SORC) for low-grade waste heat recovery.

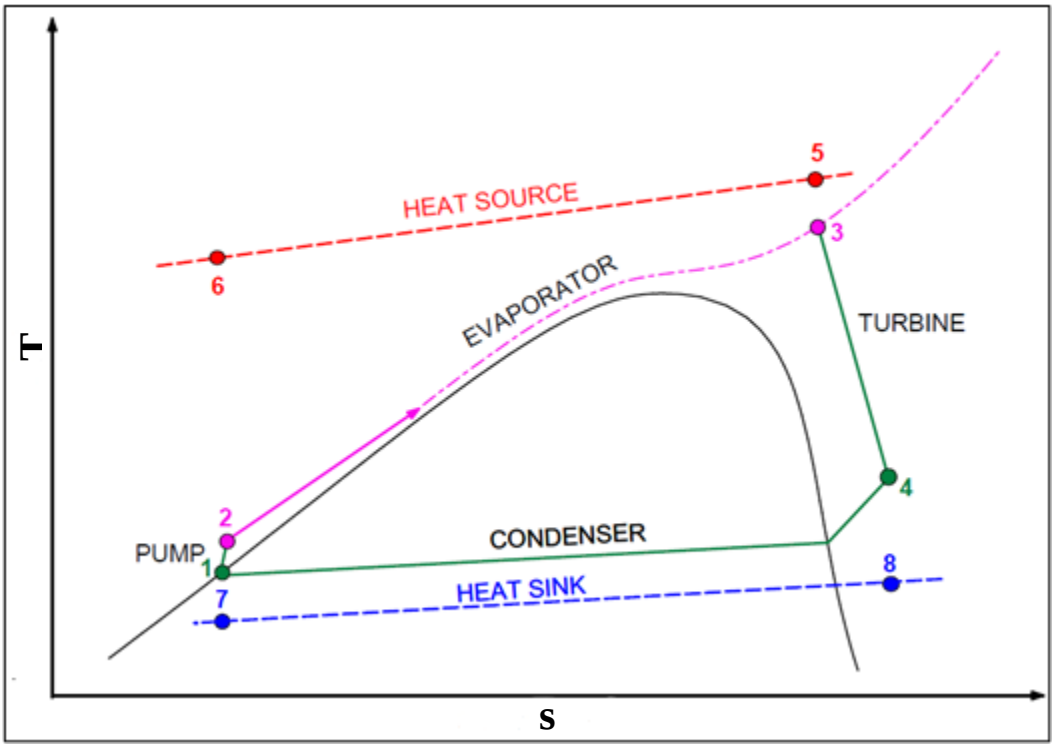

Figure 3. Temperature-Entropy (T-s) diagram for the supercritical organic Rankine cycle using Zeotropic Mixture

Most ORC uses conventional WFs, such as hydrofluorocarbons (HFCs), chlorofluorocarbons (CFCs), etc., that are harmful to the ecosystem due to environmental concerns, including high global-warming potentials (GWP) and ozone-depletion potentials (ODP). International conventions, like the Montreal Protocol with the Kigali Amendment [15][16], have banned the use of such fluids. As a result some studies have proposed using hydrocarbons (HCs) because of low GWP, zero ODP, and adequate thermodynamic performance when used as WF in a SORC [10][17][18].

On the other hand, HCs also face restrictions for use as the WF in the SORC because of their high flammability. According to the American Society of Heating, Refrigerating and Air-Conditioning Engineers (ASHRAE) safety classification, HCs are classified as A3 [19]. The flammability classification by ASHRAE is shown in Figure 4. As HCs are classified in flammability class 3, they have a higher combustion event probability and a maximum burning velocity greater than 0.1 m/s. A solution to this flammability problem is forming a zeotropic mixture of HC and carbon dioxide (CO_2) and using it as the WF for the SORC. Since CO_2 is non-flammable and environmentally friendly, mixing it with an HC will lower the fire safety concerns associated with pure HCs [14][20][21].

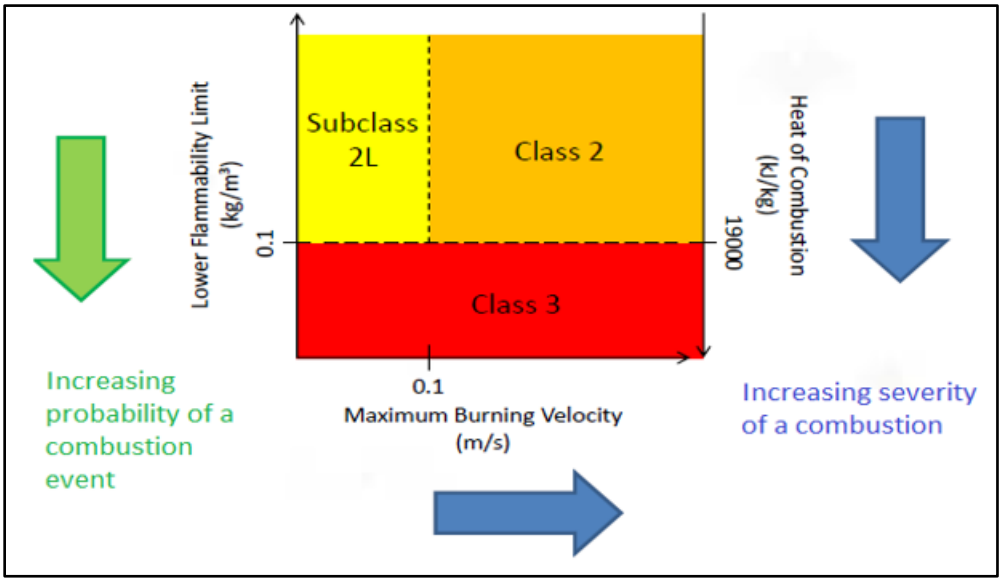

Figure 4. ASHRAE Flammability Classification

1.2. Literature Review

A detailed literature review was conducted to understand the previous research work done on the topic under consideration. The works included in this study focus mainly on the supercritical organic Rankine cycle (SORC) and the WFs used in this cycle, including zeotropic mixtures.

Mikielewicz et al. [22] conducted a study comparing different WFs for use in a SORC. The study considered six different WFs for calculations, namely R123, R141b, R134a, R365mc, ethanol, and water. A new criterion was presented in the paper to select the WF for the supercritical conditions in the cycle. Their results show R141b and ethanol as the best performing WFs for the system. The study also shows an improvement of 5% in the SORC system's efficiency compared with a subcritical ORC system.

Gao et al. [11] analyzed the performance of a SORC system based on a low-grade heat source using 18 different organic WFs. The system's performance was examined using several parameters: the net power output, exergy efficiency, expander size parameter, and heat exchanger requirement of the evaporator and the condenser. Their results showed that if the expander inlet temperature is low, then the total heat transfer requirement and the expander size are enormous. Their study recommended using R152a and R143a as suitable WFs for the system based on output and investment.

Vidhi et al. [23] presented a study on the performance analysis of a SORC based on a low-temperature geothermal source. Seven different organic WFs were considered in their study, namely R23, R32, R125, R143a, R134a, R218, and R170, and the source temperature in the study was varied between 125-200°C. The optimal WF for the system

was selected based on the energy and exergy efficiency. Their results also showed that the optimum pressure for the system is proportional to the heat source temperature with pressure increasing as temperature increases. Finally, the study concludes that R134a is the best choice for the system based on the operating conditions considered.

Chen et al. [12] conducted a study to compare the performance of a SORC based on a R134a/R32 (0.7/0.3, mass fraction) zeotropic mixture compared with an ORC based on pure R134a under the same thermal conditions. Their results showed that the SORC with zeotropic mixture had higher thermal efficiencies, compared to the ORC systems. The results also showed that using the zeotropic mixture improves the heat exchange process. Additionally, the exergy efficiency of the SORC system was higher than the ORC system. Finally, the study recommends using the zeotropic mixture in a SORC, along with a particular temperature glide in the condenser to take advantage of non-isothermal conditions.

Braimakis et al. [24] presented a study on low-grade waste-heat recovery using subcritical ORC and SORC based on natural refrigerants and their binary mixtures. Five different refrigerants and their mixtures with low global-warming and ozone-depletion potential were selected for the study. The heat source temperatures considered in the study were from 150-300°C. Their results show that using zeotropic mixtures instead of pure fluids improves the system's performance for both subcritical and supercritical conditions. The supercritical mixtures of butane-propane, butane-hexane, and butane-cyclopentane indicate the highest exergetic efficiency for low, medium, and high heat source temperature range.

Chys et al. [25] discussed the potential of using zeotropic mixtures as WFs in the ORC system. The study considered several pure organic fluids as potential components for the mixtures. A mixture selection method was discussed, and the optimal concentration of fluids in the mixture was suggested. Their results show an increase of 15.7% in the cycle efficiency and 12.3% in generated electricity for the zeotropic mixtures for a low-temperature source (150°C).

Yelishala et al. [14] conducted a study to assess the performance of a Vapor Compression Refrigeration cycle (VCRC) using binary mixtures of HC and CO_2 as WFs in order to identify the blend with the best performance for the operating conditions considered. The results identified four HC/CO_2 mixtures, namely propylene/CO_2, dimethyl ether/CO_2, propane/CO_2, and isobutane/CO_2, as the best performing WFs for the VCRC system.

Yelishala et al. [13] presented a study on the performance maximization of a VCRC system, operating on zeotropic blends of natural HCs and CO_2, based on temperature glide matching in the heat exchangers, i.e., evaporators and condensers. Their results show that the COP of the system increases by 40%, while the non-dimensional exergy destruction in the heat exchangers decreases due to temperature glide matching.

Radulovic et al. [26] performed a study of parametric optimizations of the SORC for a low-temperature geothermal heat source by using the zeotropic mixture as a WF. Their results identify the R143a/R124a mixture (0.2/0.8, mole fraction) as the optimum WF for the system based on higher thermal and exergy efficiency. Their results also reveal

that the thermal efficiency of the cycle using zeotropic mixture compositions was generally higher than the thermal efficiency of the cycle using pure component R-143a.

Wu et al. [20] conducted a study based on thermodynamic analysis and performance optimization of a SORC using CO_2-based zeotropic mixtures and operating on low-grade thermal energy. Their results identify R161/CO_2 as the best performing WF for the system based on thermal and economic performance. The results also show that the zeotropic mixture of propane and CO_2 is unsuitable for the system because of its lower thermal performance.

Shu et al. [21] presented a study based on the potential of a SORC operating on an engine's waste heat and using CO_2-based zeotropic mixtures. The thermodynamic properties of the mixtures were calculated using the Peng-Robinson equation of state. The results show that the zeotropic mixture of CO_2 and R161 (0.45/0.55, mole fraction) is the best performing WF for the system, while the zeotropic mixture of CO_2 and R32 (0.3/0.7, mole fraction) performs best when the temperature for condensation is lower than 40°C.

1.3. Objective

In this work, a zeotropic mixture of HC and CO_2 is considered as a WF for the SORC, which reduces flammability while obtaining the glide matching to improve the cycle performance. A critical factor in selecting and applying WFs for a zeotropic mixture is the effect of operating conditions (both the hot and cold source) on the cycle performance for a given setup. Several studies have been conducted to identify the optimal zeotropic mixture as the WF for the SORC based on various operating conditions; however, only a few studies considered zeotropic mixtures of HC and CO_2. This study

focuses on identifying an optimal zeotropic mixture of HC and CO_2 for a SORC system based on a low-grade heat source. The study also aims to assess the optimal zeotropic mixture's thermodynamic performance for a Houston-based facility system, using the highest and lowest annual temperature as the heat sink and dead state temperatures for the system.

2. SYSTEM DESCRIPTION AND THERMODYNAMIC ANALYSIS

2.1. System Description

The WFs considered in this study include dimethyl ether (DME), R1234yf, diethyl ether (DEE), isobutane, and CO_2. These WFs, along with their thermal and environmental characteristics, are listed in Table 1 [27]. The ASHRAE Safety Group for all the WFs is obtained from ASHRAE Standard 34 [19], which also assigns to all refrigerants a reference letter and a reference number based on the hazards involved in their use. For example, the reference letter indicates the toxicity class of the refrigerant, while the reference number designates the flammability of the refrigerant. The WFs used in this study herein are classified into toxicity class A, indicating lower toxicity. Flammability is categorized into three classes, i.e., non-flammable (class 1), lower flammability (class 2), and higher flammability (class 3). There is a subclass 2L of flammability class 2, which indicates that the refrigerants burn very slowly.

Table 1. List of Fluids with their Relevant Properties and Characteristics [10]

Fluid Name	Tc (K)	Pc (kPa)	GWP	Flammability	ASHRAE Safety Group
Dimethyl Ether	400	5367	1	High	A3
R1234yf	368	3382	<1	Low	A2L
Isobutane	407	3640	3	High	A3
Diethyl Ether	467	3644	4	-	-
Carbon Dioxide	304	7377	1	No Flame Propagation	A1

The system considered in this study (shown in Figure 3) utilizes various low-grade heat sources with evaporator inlet temperatures (T_5) varying from 400 K to 500 K. The heat sink (i.e., cold water) for the system is assumed to be at the dead state, i.e., at an ambient temperature and pressure of 300 K and 101.325 kPa, respectively, for all cases. There are four major components used in the system: a pump, an evaporator, a turbine, and a condenser. In Figures 2 and 3, the WF at a saturated-liquid state is first pumped to a high-pressure P_2 by a pump, and then the WF is heated to a high-temperature T_3 by a low-grade heat source at temperature T_5 in a shell-and-tube heat exchanger (evaporator). The WF at a supercritical state is then expanded to the condenser pressure P_4 in the turbine and generates a fixed turbine power output of 250 kW. The WF is then condensed back to the saturated-liquid state at temperature T_1 by a condenser. The temperature difference between the heat source and the WF in the evaporator (i.e., $\delta T_1 = T_5 - T_3$), and the temperature difference between the WF and the heat sink in the condenser (i.e., $\delta T_2 = T_1 - T_7$), is assumed as 10 K.

2.2. Thermodynamic Analysis

The energy and exergy analyses of the cycle were performed by using several PYTHON scripts for pure fluids and zeotropic mixtures. The thermophysical properties of the WFs, such as enthalpy, entropy, and other thermodynamic properties, at specified cycle operating conditions were computed by using the Engineering Equation Solver (EES) for pure WFs and REFPROP by the National Institute of Standards and Technology (NIST) for Zeotropic Mixture, with both combined using PYTHON through an interface. Zeotropic mixtures in REFPROP are found from a function, that produces a blend of various WFs on either a molar or mass concentration basis. For this study, the zeotropic mixtures are developed on a molar concentration basis.

Certain assumptions are made to simplify the system analysis and calculations in this study including [10]:

1. The cycle operates at steady-state conditions.
2. Pressure losses in the evaporator, condenser and piping system are neglected.
3. The isentropic efficiency of the pump and turbine is assumed to be 80% and 85%, respectively.
4. The hot air entering the evaporator at point 5 is assumed as the heat source with a constant flow rate of $\dot{m}_5$ = 20 kg/s.
5. The cold water entering the condenser at point 7 is assumed as the heat sink with a constant flow rate of $\dot{m}_7$ = 10 kg/s.

Uncertainty analysis was performed for cycle operation based on pure WFs for the uncertainties assumed in the cycle inlet parameters using EES, as shown in Table 2 [10].

Uncertainty analysis was not conducted for the case of zeotropic mixtures due to complex computations.

Table 2. Uncertainty assumptions of the measured variables [10]

Parameters	**Uncertainty Assumption**
Temperature differences between WF and the heat source in the evaporator, δT_1	1 K
Temperature differences between WF and the cold sink in the condenser, δT_2	1 K
Isentropic Efficiency of Pump	0.2 %
Isentropic Efficiency of Turbine	0.2 %
Interest Rate, i_r	0.1 %
Dead State Temperature, T_0	1 K
Dead State Pressure, P_0	0.1 %
Heat Source Temperature, T_5	1 K
Heat Source Pressure, P_5	0.1 %
Heat Sink Temperature, T_7	1 K
Heat Sink Pressure, P_7	0.1 %
Flow rate of hot air in the evaporator, m_5	0.2 kg/s
Flow rate of cold water in the condenser, m_7	0.1 kg/s

2.2.1. Energy Analyses

Energy analyses of the SORC system (shown in Figures 2 and 3) for different WFs were conducted to investigate the system's performance under given operating conditions based on the first law of thermodynamics. The fundamental thermodynamic relations used to perform the analyses are obtained from standard thermodynamics textbooks [28] [29].

2.2.1.1. Cycle Efficiency

The cycle efficiency for the system is defined as the ratio of net work output of the cycle and heat input to the cycle from a low-grade heat source as follows,

$$\eta = \frac{\dot{W}_{net}}{\dot{Q}_{in}} \times 100 \tag{1}$$

where, $\dot{W}_{net}$ represents the net work output of the cycle.

$$\dot{W}_{net} = \dot{W}_t - \dot{W}_p \tag{2}$$

and $\dot{W}_t$ represents the power generated by the turbine, $\dot{W}_p$ represents the power consumed by the pump, and $\dot{Q}_{in}$ is the heat input to the cycle from a low-grade heat source. The above energy transfers are obtained using the following expressions based on energy balance solutions,

$$\dot{W}_t = \dot{m} \times (h_3 - h_4) \tag{3}$$

$$\dot{W}_p = \dot{m} \times (h_2 - h_1) \tag{4}$$

$$\dot{Q}_{in} = \dot{m}_{hs} \times (h_5 - h_6) \tag{5}$$

where, h is the specific enthalpy of the WF at a particular state point, $\dot{m}$ is the mass flow rate of the WF, and $\dot{m}_{hs}$ is the mass flow rate of the low-grade heat source. The heat output from the condenser is given by,

$$\dot{Q}_{out} = \dot{m}_{cs} \times (h_8 - h_7) \quad (6)$$

where the subscript cs indicates the cold source. In this study, a shell-and-tube type heat exchanger is considered as the evaporator, which is modeled using the following expression [10],

$$\dot{Q} = U_e \times A_e \times \Delta T_{LMTD} \quad (7)$$

where, A_e indicates the area of the evaporator. The overall heat transfer coefficient (U_e) for the shell-and-tube type heat exchanger (evaporator) is assumed to be 0.3 kW/m^2-K [30], [31]. The logarithmic mean temperature difference, ΔT_{LMTD} for the heat exchanger, is given by,

$$\Delta T_{LMTD} = \frac{((T_5 - T_3) - (T_6 - T_2))}{\ln\left(\frac{(T_5 - T_3)}{(T_6 - T_2)}\right)} \quad (8)$$

2.2.1.2. Volumetric Power Coefficient

Similar to the volumetric refrigeration capacity (VRC) for system sizing in Refrigeration Systems, a volumetric power coefficient (VPC) is introduced in this study, defined as the ratio of turbine output power and volume flow rate of the WF at the turbine's inlet. It is expressed as [10],

$$VPC = \frac{\dot{W}_t}{\dot{m} \times v_{in}} \quad (9)$$

where, v_{in} is the specific volume at the turbine's inlet. VPC is used to interpret the size of the system based on work output for different WFs. The mass flow rate of the WF ($\dot{m}$) is calculated by,

$$\dot{m} = \frac{\dot{W}_t}{(h_3 - h_4)} \quad (10)$$

2.2.2. Exergy Analyses

The exergy analyses of the SORC system, shown in Figures 2 and 3, were performed using the second law of thermodynamics for the purposes of identifying the effects of system irreversibilities, which decreases the cycle efficiency during each process. The specific exergies at a state point i in the system is given by the following expression,

$$ex_i = \left((h_i - h_0) - T_0(s_i - s_0)\right) \tag{11}$$

where, h_i and s_i represents the enthalpy and entropy at the specific state point, respectively. Also, T is temperature, while subscripts i denotes the specific state point, and o denotes the ambient condition.

2.2.2.1. Exergy Efficiency

The exergy efficiency of the system is defined as the ratio of net work output of the cycle and exergy input to the cycle from a low-grade heat source as follows,

$$\eta_s = \frac{\dot{W}_{net}}{\dot{Q}_{in} \times \left[1 - \frac{T_0}{T_3}\right]} \times 100 \tag{12}$$

where, T_3 is the temperature of the WF at the outlet of the evaporator.

2.2.2.2. Exergy Destruction

Exergy destruction is defined as the amount of exergy destroyed during a process due to irreversibilities and represents the lost work potential [32]. The exergy destruction in each of the four components of the SORC system, i.e., the pump (p), the evaporator (e), the turbine (t), and the condenser (c), are computed using the following expressions [10],

$$\dot{XD}_p = \dot{W}_p + \dot{m} \times (ex_1 - ex_2)\ , \tag{13}$$

$$\dot{XD}_e = \dot{Q}_{in} \times \left[1 - \frac{T_0}{T_3}\right] + \dot{m} \times (ex_2 - ex_3)\ , \tag{14}$$

$$\dot{XD}_t = \dot{m} \times (ex_3 - ex_4) - \dot{W}_t\ , \tag{15}$$

$$\dot{XD}_c = \dot{m} \times (ex_4 - ex_1) - \dot{Q}_{out} \times \left[1 - \frac{T_4}{T_0}\right] \tag{16}$$

where, T represents the temperature at a particular state point i. The total exergy destruction of the system is defined as the sum of exergy destruction in all four system components as follows,

$$\dot{XD}_{Total} = \dot{XD}_p + \dot{XD}_e + \dot{XD}_t + \dot{XD}_c \tag{17}$$

The non-dimensional exergy destruction in the condenser and evaporator is defined as the ratio of the component's exergy destruction and the exergy input to the cycle from the low-grade heat source. It is given by [10],

$$\lambda_k = \frac{\dot{XD}_k}{\dot{Q}_{in} \times \left[1 - \frac{T_0}{T_3}\right]} \tag{18}$$

where subscript k represents the system component, i.e., condenser or evaporator. The total non-dimensional exergy destruction of the system is defined as the ratio of the system's total exergy destruction and the exergy input to the cycle from the low-grade heat source as follows,

$$\lambda_{Total} = \frac{\dot{XD}_{Total}}{\dot{Q}_{in} \times \left[1 - \frac{T_0}{T_3}\right]} \tag{19}$$

2.2.3. Exergoeconomic Analysis

The exergoeconomic analysis of the cycle is conducted for the cases of pure WFs to obtain the cost of net work (in $/MWh) and total cost of exergy destruction (in $/h) in the system. The analysis is not performed for zeotropic mixtures due to the complexity

involved in its computations. The analysis performed in this study is based on the specific exergy costing method (SPECO), which was introduced by Lazzaretto et al. [33]. For each system component, the cost balance equations, along with its auxiliary equations and purchased equipment cost (PEC) equations, are presented in Table 3 [34], where $\dot{C}_i$ is the cost rate at state point i, and c_i is the cost per unit exergy at state point i.

Table 3. Cost balance equations, associated auxiliary equations, and purchased cost equations of components for the system considered [10][34]

Component	Cost Balance Equation	Auxiliary Equation	Purchased Cost
Pump	$\dot{C}_1 + \dot{C}_{W,pump} + \dot{Z}_{pump} = \dot{C}_2$	$c_1 = c_2$ $c_1 = known$	$PEC_{pump} = 3540 \times \left(\dot{W}_{pump}\right)^{0.71}$
Evaporator	$\dot{C}_5 + \dot{C}_2 + \dot{Z}_{evap} = \dot{C}_6 + \dot{C}_3$	$c_5 = c_6$	$PEC_{evap} = 130 \times \left(\frac{A_{evap}}{0.093}\right)^{0.78}$
Turbine	$\dot{C}_3 + \dot{Z}_{turb} = \dot{C}_4 + \dot{C}_{W,turb}$	$c_3 = c_4$	$PEC_{turb} = \left(\frac{1536\dot{m}_f}{0.92-\eta_T}\right) \times \{\ln(\theta)\} \times \left(1 + e^{\left((0.036T_4)-54.4\right)}\right)$
Condenser	$\dot{C}_4 + \dot{C}_7 + \dot{Z}_{cond} = \dot{C}_1 + \dot{C}_8$	$c_1 = c_4$	$PEC_{cond} = 1773 \times \left(\dot{m}_f\right)$

The term $\dot{Z}$ in Table 3 indicates the total cost rate associated with each system component, including the purchase, operation, and maintenance costs. It is expressed as [34],

$$\dot{Z} = \frac{(PEC)\times(CRF)\times\phi}{3600\times N} \tag{20}$$

where, ϕ denotes the maintenance factor, which is assumed as 1.1 in this research, while N indicates the annual operating hours, which is assumed to be 8760 hours. The term CRF

in Equation 20 represents the Capital Recovery Factor, which is given by the following equation [34],

$$CRF = \frac{i_r(1+i_r)^n}{(1+i_r)^n-1} \tag{21}$$

where, i_r is the interest rate, assumed to be 12%, while n represents the system's lifetime, which is assumed as 20 years in this research.

The cost rate associated with the fuel and product for each system component can be computed by using the fuel and product concepts in the SPECO method. According to this method, the fuel refers to all the exergy added to the components, while the product is defined as all the exergy removed from the components [33]. The following expressions are used to calculate the cost rate associated with the fuel and product, along with the cost rate associated with the exergy destruction in each component, k [35],

$$\dot{C}_{P,k} = c_{P,k} \times \dot{E}_{P,k} \tag{22}$$

$$\dot{C}_{F,k} = c_{F,k} \times \dot{E}_{F,k} \tag{23}$$

$$\dot{C}_{XD,k} = c_{F,k} \times \dot{X}D_k \tag{24}$$

where, $c_{P,k}$ and $c_{F,k}$ denotes the cost per unit exergy of the component's product and fuel, respectively, while $\dot{E}_{P,k}$ and $\dot{E}_{F,k}$ represents the product and fuel's exergy rate respectively for the kth component.

The unit cost of the net work ($/MWh) is determined by using the following expression [33],

$$c_{W,net} = \frac{\dot{C}_{W,turb}-\dot{C}_{W,pump}}{\dot{W}_{turb}-\dot{W}_{pump}} \tag{25}$$

where, $\dot{C}_{\dot{W},turb}$ indicates the unit cost of power generated by the turbine and $\dot{C}_{\dot{W},pump}$ represents the unit cost of power consumed by the pump.

2.2.4. Thermodynamic Databases

In this study, the analysis conducted for pure WFs is computed using the thermophysical properties of the WFs obtained from the EES database, which uses the fundamental equation of state for calculating properties. The analysis conducted for zeotropic mixtures is computed using the thermophysical properties of the mixtures obtained from REFPROP, which uses the NIST database for calculating properties. Therefore, it is necessary to compare the results from both databases.

Figure 5 shows the variation in cycle efficiency (η) for different heat source inlet temperatures (T_5) when the reduced pressure (θ), which is defined as the ratio of evaporator pressure and WF's critical pressure, is varied from one to four. The solid lines demonstrate the results obtained using the EES database, while the dashed lines demonstrate the results obtained using the REFPROP database. The results obtained in Figure 5 show that both the databases (i.e., EES and REFPROP) have similar cycle efficiency trends with different values due to different Equations of State by different databases. The differences between the cycle efficiency values from the EES and REFPROP are insignificant, meaning that we can conclude that the findings from results obtained from the EES database also hold for the findings from results obtained from the REFPROP database.

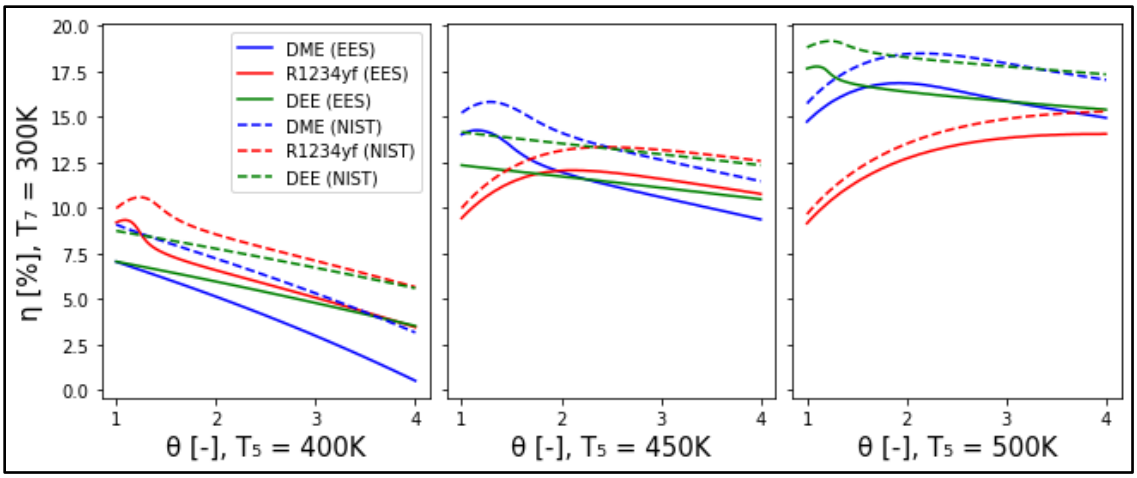

Figure 5. Cycle efficiency (η) variation with reduced pressure (θ) for screened working fluids for different heat-source temperature T_5 obtained from different thermodynamic databases

3. PERFORMANCE OF HYDROCARBONS AS WORKING FLUID FOR A SIMPLE SUPERCRITICAL ORGANIC RANKINE CYCLE

The performance of the system shown in Figure 2 is studied for the four WFs, namely DME, R1234yf, DEE, and isobutane, at different heat-source inlet temperatures (T_5) with variations in evaporator pressure (P_2) above the critical pressure (P_c) of each WF. The reduced pressure (θ), defined as the ratio of evaporator pressure and WF's critical pressure, is an essential factor in the analysis due to extra heat transfer challenges that occur when operating in the pseudocritical region of the WF. The reduced pressure (θ) is varied from one to four, while the heat-source inlet temperature is varied from 400 K to 500 K. The thermophysical properties of the WFs were computed using the EES. The cycle's performance is analyzed based on cycle efficiency, VPC, non-dimensional exergy destruction, and exergoeconomics.

3.1. Cycle Efficiency

Figure 6 shows the impact of variations of reduced pressure (θ) on the cycle efficiency (η) at different heat source inlet temperatures (T_5) for all the WFs. At a heat-source inlet temperature of 400 K, R1234yf shows cycle performances better than other WFs with a maximum cycle efficiency of 9.7% at a reduced pressure of θ = 1.09 (3686 kPa). At 450 K, DME shows a cycle performance better than other WFs for reduced pressure values less than 1.94 with a maximum cycle efficiency of 14.7% at a reduced pressure of θ = 1.15 (6183 kPa). It is interesting to note that at the reduced pressure value of 1.94, all the WFs demonstrate similar cycle performances. For reduced pressure values

higher than 1.94, R1234yf shows cycle performances better than other WFs. In contrast, at 500 K, both DME and DEE show cycle performances better than other WFs, with a maximum cycle efficiency of 17.9% obtained for DEE at a reduced pressure of θ = 1.09 (3975 kPa).

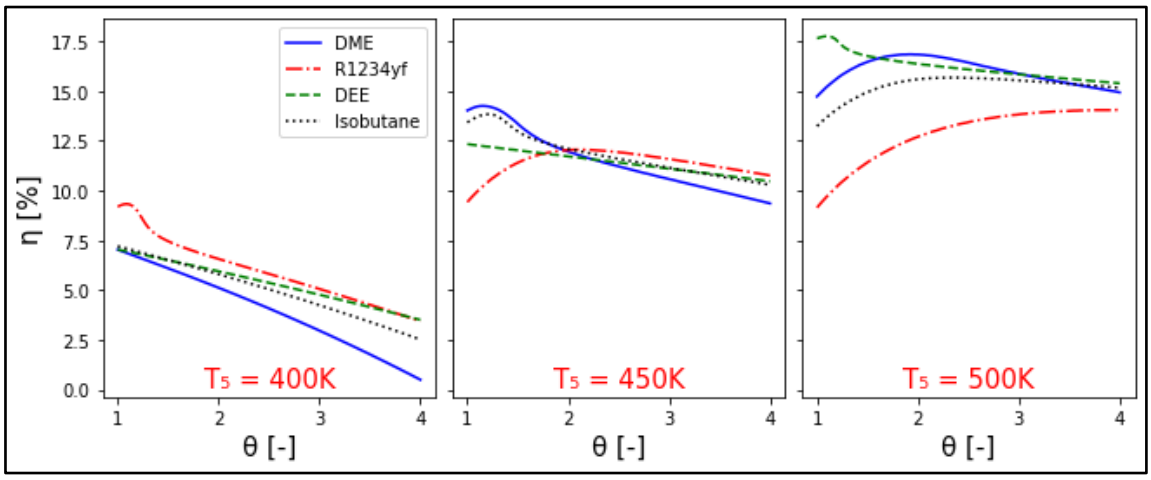

Figure 6. Cycle efficiency (η) variation with reduced pressure (θ) for screened working fluids for different heat-source inlet temperatures T_5 [10]

The results obtained from Figure 6 are important for analyzing the performances of all the WFs, but it does not provide a clear picture of performance in terms of absolute operating pressures of the cycle. Therefore, the critical pressure of CO_2 has been selected as a reference for this purpose in this study. As an alternative normalized parameter, the normalized reduced pressure (ϕ) is then defined as the ratio of evaporator pressure (P_2) to the critical pressure of CO_2 (7377 kPa). The impact of variations of normalized reduced pressure (ϕ) on the cycle efficiency (η) at different heat-source inlet temperatures (T_5) for all the WFs is shown in Figure 7. The normalized reduced pressure (ϕ) range is taken from half to three. For a heat-source inlet temperature of 400 K, all the WFs demonstrate

decreasing efficiency trend with a rise in normalized reduced pressure. The maximum cycle efficiency at 400 K is obtained for R1234yf (9.7%) at $\phi = 0.5$. At 450 K, DME shows a superior performance compared to other WFs with a maximum cycle efficiency of 14.7% at $\phi = 0.84$. At 500 K, DEE initially shows a cycle performance better than other WFs for lower values of ϕ with a maximum cycle efficiency of 17.9% at $\phi = 0.54$, while DME shows a cycle performance better than other WFs at higher values of ϕ. The vital observation from Figure 7 is that the DME is a suitable WF for the system, due to superior cycle performance, when the heat-source inlet temperature varies from 400 K to 500 K.

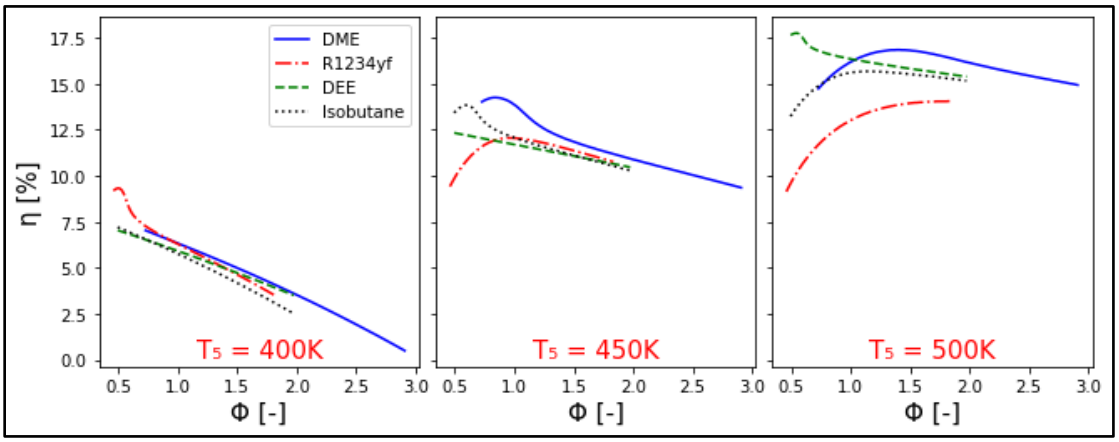

Figure 7. Cycle efficiency *(η)* variation with normalized reduced pressure *(ϕ)* for screened working for different heat-source inlet temperatures T_5 [10]

3.2. Volumetric Power Coefficient

VPC may be used to interpret the size of the system in terms of work output for different WFs [10]. A higher value of VPC is desirable for the WF, as it indicates that the system produces the same power output with less volume flow of the WF at the turbine inlet. Figures 8 and 9 show the impact on the VPC of varying reduced pressure (θ) and normalized reduced pressure (ϕ) at different heat-source inlet temperatures (T_5) for all the

WFs. The trends obtained in Figures 8 and 9 show that the VPC increases with a rise in pressure for all heat-source inlet temperatures. For a heat-source inlet temperature of 450 K, DME and DEE have the same VPC at a reduced pressure of 3.64; however, at the same heat-source inlet temperature in Figure 9, the same VPC for DME is not reached until a higher value of ϕ. The results obtained from Figures 8 and 9 indicate the superiority of DEE in terms of system sizing followed by DME.

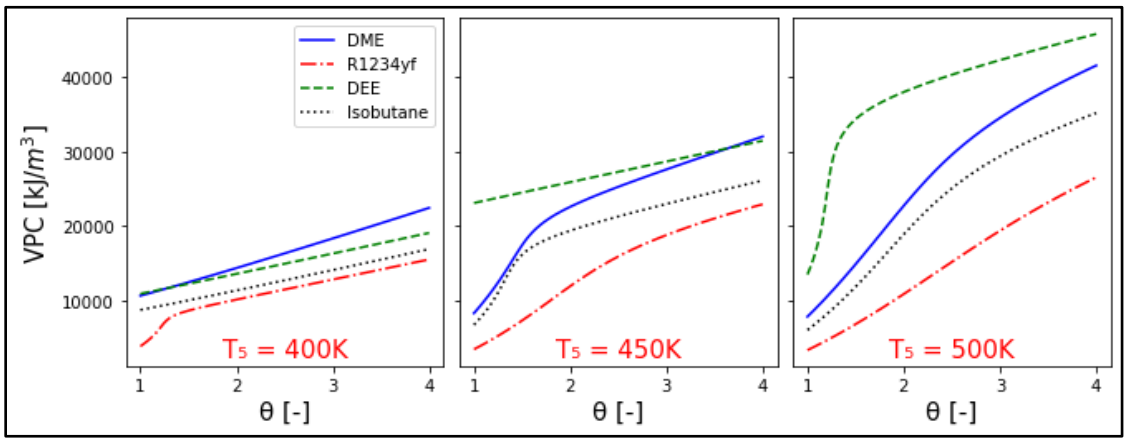

Figure 8. Volumetric power coefficient *(VPC)* variation with reduced pressure *(θ)* for different heat-source inlet temperatures T_5 [10]

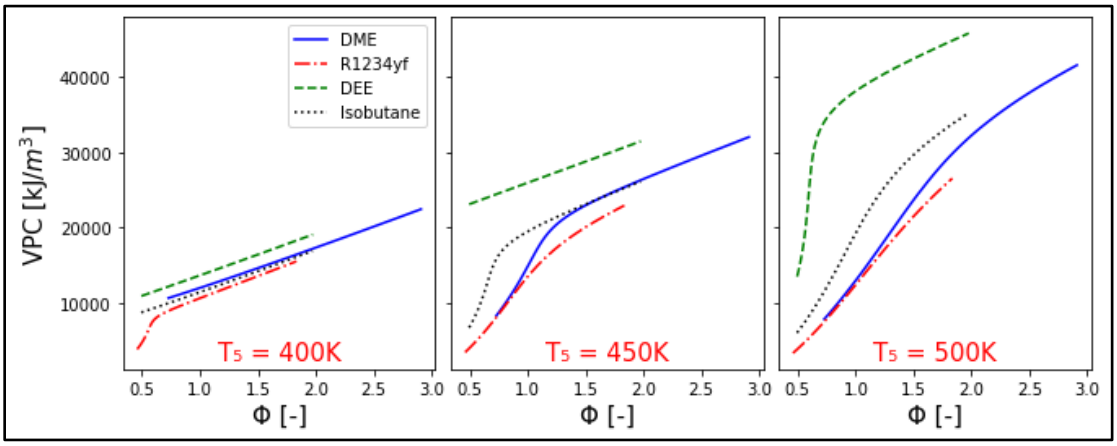

Figure 9. Volumetric power coefficient *(VPC)* variation with normalized reduced pressure *(ϕ)* for different heat-source inlet temperatures T_5 [10]

3.3. Non-Dimensional Exergy Destruction

The non-dimensional exergy destruction (λ) in a component is defined as the ratio of the component's exergy destruction and the exergy input to the cycle from the low-grade heat source. The lower value of λ indicates efficient utilization of the energy available in the low-grade heat source, resulting in cost-effective systems. The exergy destruction in each cycle component of the SORC system was calculated for all the WFs considered in this study, using Equations 13, 14, 15, and 16, at different heat-source inlet temperatures (T_5) and reduced pressure (θ). The data obtained from these computations showed that the evaporator and condenser have the maximum exergy destruction, compared to that of other components. The non-dimensional exergy destruction (λ) in the evaporator and condenser was then calculated using Equation 18, and the results were plotted as shown in Figures 10 and 11 as a function of reduced pressures and heat-source inlet temperatures.

The trends shown in Figure 10 can be used to evaluate the variations of heat input to the cycle from low-grade heat source ($\dot{Q}_{in}$) and the change in exergy at the inlet and outlet of the evaporator, as given in Equations 13 and 18. For a heat-source inlet temperature of 400 K, R1234yf initially shows the lowest non-dimensional exergy destruction in the evaporator for reduced pressure values less than 1.94. At a reduced pressure of 1.94, R1234yf reaches its peak value of 0.35, after which DME exhibits the lowest non-dimensional exergy destruction in the evaporator. The highest non-dimensional exergy destruction trends at 400 K are obtained for DEE. At 450 K and 500

K, DME shows the lowest non-dimensional exergy destruction in the evaporator, while DEE shows the highest non-dimensional exergy destruction compared to other WFs.

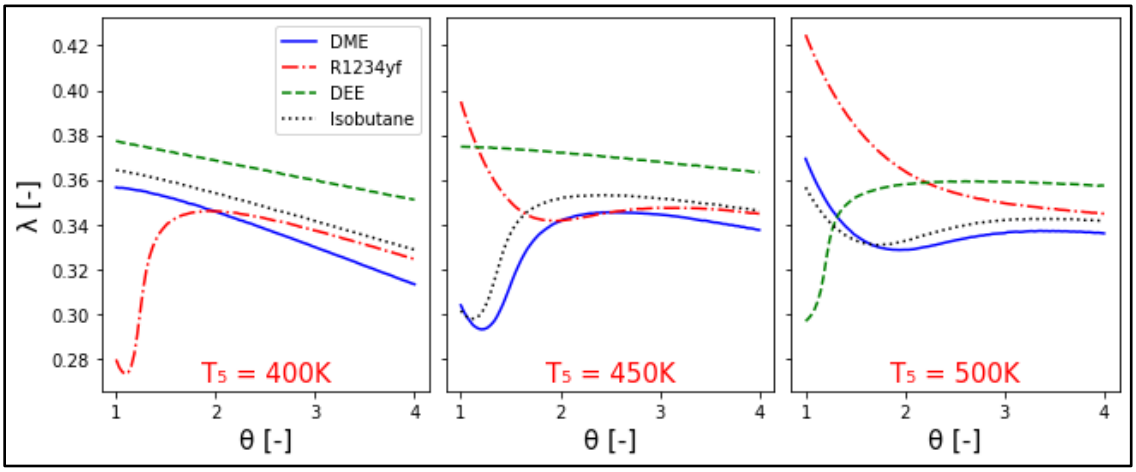

Figure 10. Variation of non-dimensional exergy destruction *(λ)* in the evaporator with reduced pressure *(θ)* for different heat-source inlet temperatures T_5 [10]

The trends shown in Figure 11 can be used to evaluate the variations in heat input to the cycle ($\dot{Q}_{in}$), the heat output from the condenser ($\dot{Q}_{out}$), and the change in exergy at the inlet and outlet of the condenser, as given in Equations 16 and 18. For a heat-source inlet temperature of 400 K, all the WFs show approximately constant (with ± 4% variations) non-dimensional exergy destruction of 0.30. At 450 K and 500 K, all the WFs demonstrate a decreasing trend of non-dimensional exergy destruction in the condenser, with R1234yf having the highest non-dimensional exergy destruction. Therefore, R1234yf is not a suitable choice as a WF at heat-source inlet temperatures of 450 K and 500 K. It is evident from Figures 10 and 11 that at reduced pressure values, $\theta > 2$, all the WFs demonstrate a decreasing trend of non-dimensional exergy destruction in the evaporator and condenser.

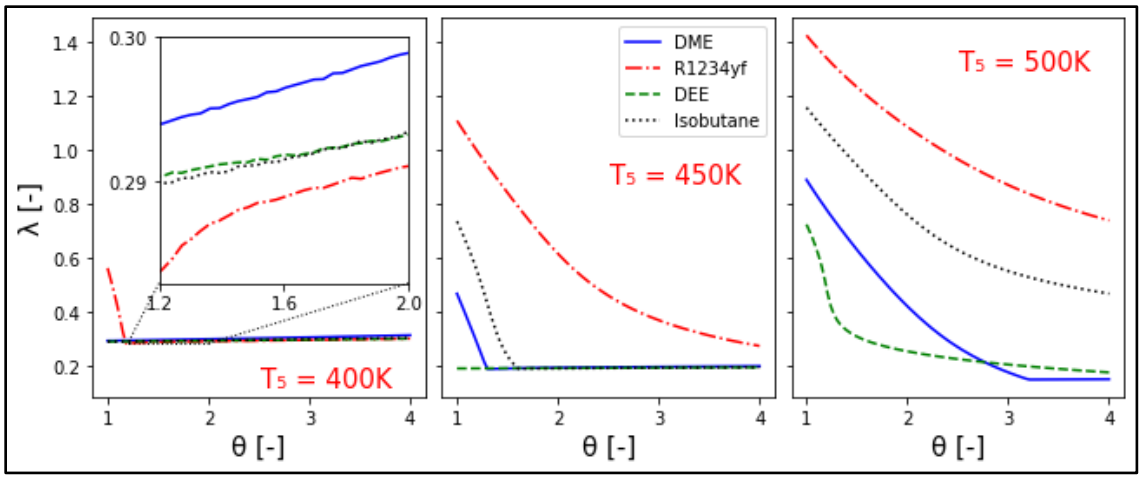

Figure 11. Variation of non-dimensional exergy destruction *(λ)* in the condenser with reduced pressure *(θ)* for different heat-source inlet temperatures T_5 [10]

The results obtained in Figures 10 and 11 are based on an evaporator fluid-temperature difference (δT_1) of 10 K. Figure 12 shows the exergy destruction in each cycle component for all the WFs considered in this study at a reduced pressure value of $\theta = 2$ and different temperature differences of 5 K, 10 K, and 20K. This figure also shows the total exergy destruction in the system for all the WFs at different heat-source inlet temperatures (T_5) and evaporator fluid-temperature differences (δT_1). For a heat-source inlet temperature of 400 K, the total exergy destruction in the system for DME and DEE decreases by 3.3% and 2.1%, respectively, when δT_1 is increased from 5 K to 20 K. At 450 K, the total exergy destruction in the system for DEE decreases by 14.2%, while the total exergy destruction in the system for DME increases by 3.0%, when δT_1 is increased from 5 K to 20 K. At 500 K, the total exergy destruction in the system for DME and DEE decreases by 15.8% and 15.4%, respectively, when δT_1 is increased from 5 K to 20 K. The important conclusion drawn from Figure 12 is that DME is the most suitable WF for all

the operating conditions considered in this study. Hence, DME is chosen for exergoeconomic analysis.

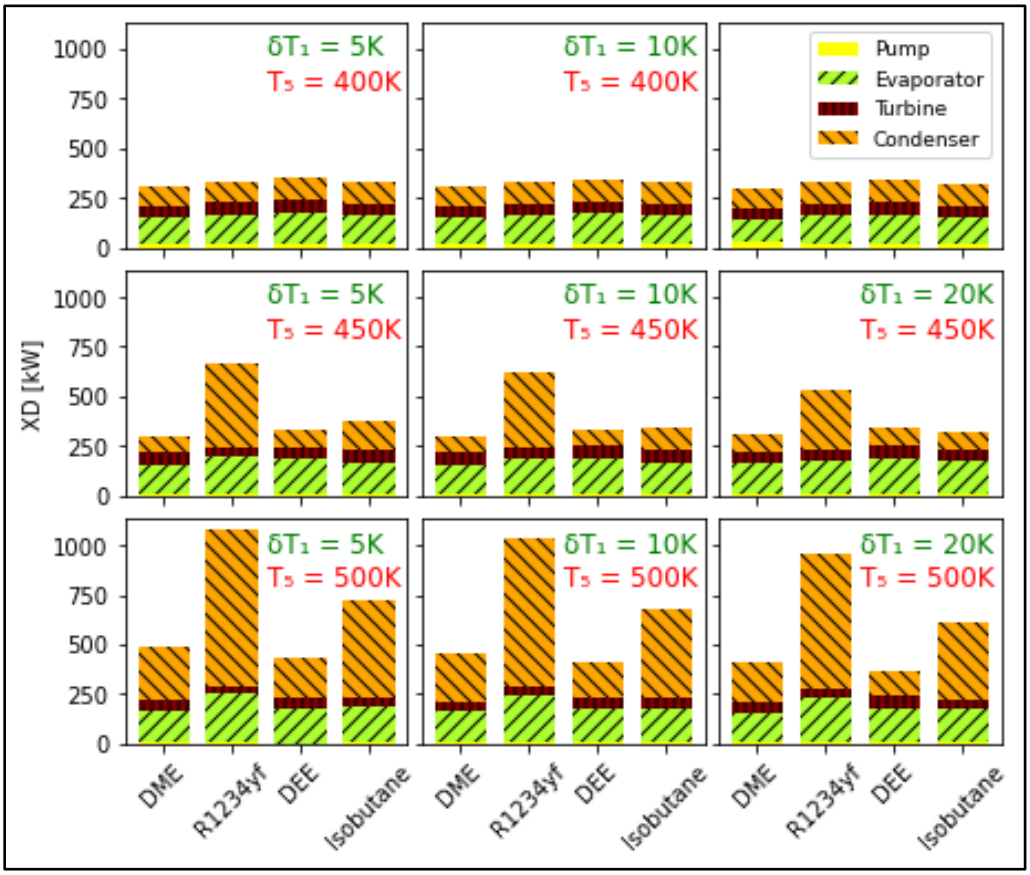

Figure 12. Variation of exergy destruction ($\dot{X}D$) in individual components for different heat-source inlet temperatures T_5 and evaporator temperature difference (δT_1) [10]

3.4. Exergoeconomics

The exergoeconomic analysis in this study is performed using a methodology based on the Specific Exergy Costing (SPECO) method. As observed in Figures 10 and 11, the exergy destruction of the WFs was found to be optimal at a reduced pressure value, $\theta = 2$. Therefore, the exergoeconomic analysis is conducted for DME and isobutane at $\theta = 2$ and heat-source inlet temperatures (T_5) of 400 K, 450 K, and 500 K. The results

obtained for this analysis are presented in Table 4. For heat-source inlet temperature of 450 K and 500 K, the unit exergetic cost of net work ($/MWh) and the total cost of exergy destruction in the system ($/h) for DME is lower than the costs for isobutane. At 400 K, the unit exergetic cost of net work and the total cost of exergy destruction for DME are higher than that for isobutane; however, the difference between the values is insignificant.

Table 4. Cost analysis for DME and isobutane at a heat source temperature of 400 K, 450 K, and 500 K [10]

Parameters	400 K		450 K		500 K	
	DME	**Isobutane**	**DME**	**Isobutane**	**DME**	**Isobutane**
Net Work (kW)	**104.7±4.6**	**124.5±4.3**	**182.6±1.9**	**192.5±1.6**	**210.9±0.7**	**214.9±0.6**
Pump Work ($/h$)	2.38±0.10	2.41±0.09	0.87±0.03	0.89±0.03	0.39±0.01	0.45±0.01
Turbine Work ($/h$)	12.31±0.03	13.65±0.04	11.67±0.02	12.95±0.03	11.19±0.02	12.25±0.02
Net Work Cost ($/h$)	**9.93±0.07**	**11.24±0.05**	**10.80±0.03**	**12.06±0.02**	**10.80±0.02**	**11.80±0.02**
Net Work Cost ($/MWh$)	**94.94±3.54**	**90.27±2.45**	**59.18±0.49**	**62.64±0.45**	**51.25±0.17**	**54.94±0.15**
$C_{XD,C}$ (%)	38.5±4.0	50.0±5.0	32.0±3.3	38.7±3.1	60.0±1.3	72.4±0.6
$C_{XD,E}$ (%)	33.6±2.7	16.7±7.3	42.2±1.9	39.4±1.8	26.5±0.8	19.7±0.4
$C_{XD,P}$ (%)	3.7±0.2	4.4±0.5	1.5±0.1	1.2±0.1	0.4±0.0	0.3±0.0
$C_{XD,T}$ (%)	24.0±1.4	28.9±3.7	24.3±1.4	20.7±1.3	13.1±0.6	7.7±0.3
Total Cost$_{XD}$ ($/h$)	**9.03±0.49**	**8.36±1.05**	**8.92±0.48**	**11.56±0.57**	**14.59±0.54**	**25.04±0.65**

The cost rate of exergy destruction in each cycle component for DME and isobutane are shown in Figure 13 at a reduced pressure value of θ = 2, for different heat-source inlet temperatures (T_5). The results show that the pump has the lowest cost rate of exergy destruction, while the evaporator and the condenser have the highest cost rate of exergy destruction. At a heat-source inlet temperature of 400 K, the difference between the total cost of exergy destruction for DME and isobutane is negligible. At 450 K and 500K, the total cost of exergy destruction for DME is calculated to be 8.92 ± 0.48 $/h and 14.59 ± 0.54 $/h, while it is calculated to be 11.56 ± 0.57 $/h and 25.04 ± 0.65 $/h for isobutane. Hence DME is selected as a potential WF for the system based on exergoeconomic analysis.

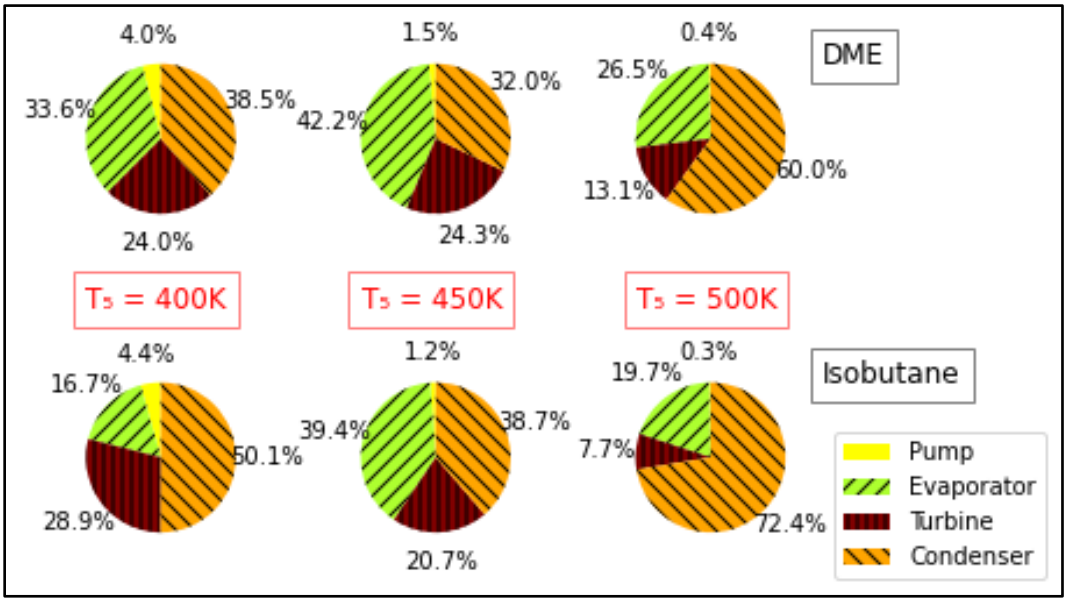

Figure 13. Cost rate of exergy destruction in individual cycle components for different heat source inlet temperatures T_5 for (top) DME, (bottom) isobutane [10]

In summary, based on energy, exergy, and exergoeconomic analysis, DME is the suitable choice as a WF for SORC for those operating conditions considered in this study.

4. PERFORMANCE OF HYDROCARBON-CO_2 ZEOTROPIC BLENDS FOR A SUPERCRITICAL ORGANIC RANKINE CYCLE

A zeotropic mixture is defined as a mixture of two WF components with different boiling points. The phase change in a zeotropic mixture occurs across a range of temperatures for any given pressure [36], [37]. The liquid and vapor phases of pure fluids have the same saturation temperatures; in contrast, the liquid and vapor phases for zeotropic mixtures have different saturation temperatures, as shown in Figure 14. The saturated-liquid temperatures for the DME-CO_2 zeotropic mixture at 50% CO_2 concentration are shown by blue lines, while the saturated-vapor temperatures are shown by red lines. The saturated-liquid and saturated-vapor temperatures for pure fluids are shown by black lines for DME and CO_2. The circles represent the critical condition for the working fluid.

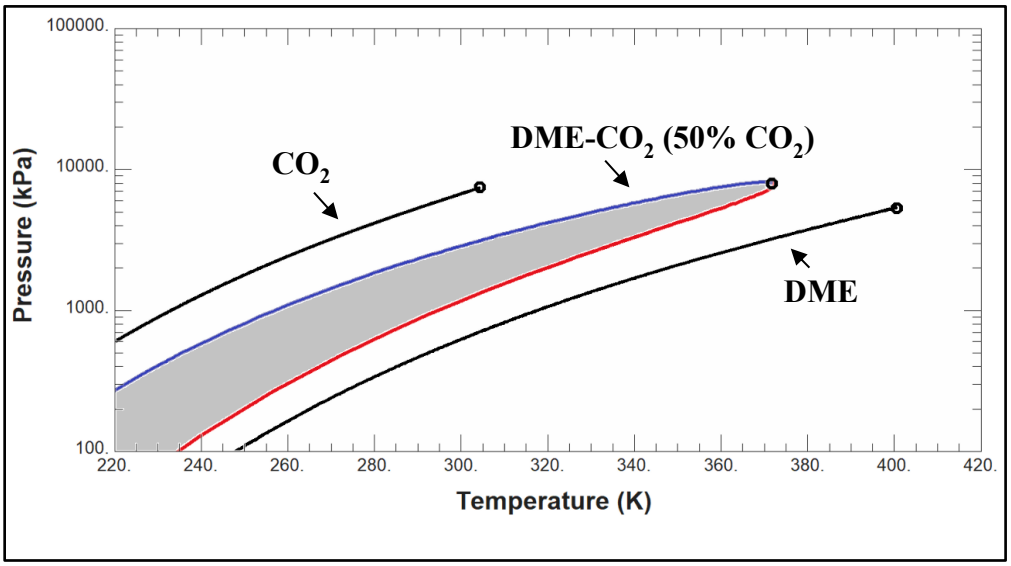

Figure 14. Pressure-Temperature diagram for pure DME, CO_2, and DME-CO_2 zeotropic mixture

Figure 15 shows a 3D phase diagram for a DME-CO_2 zeotropic mixture, illustrating saturated liquid and vapor temperatures at different CO_2 concentrations varying from 0% to 100%. As before, the saturated-liquid temperatures are shown by blue lines, while the red lines show the saturated-vapor temperatures for the DME-CO_2 zeotropic mixture. Again, black lines show saturated-liquid and saturated-vapor temperatures for pure DME and CO_2. The green-colored circles represent the critical condition for the fluid.

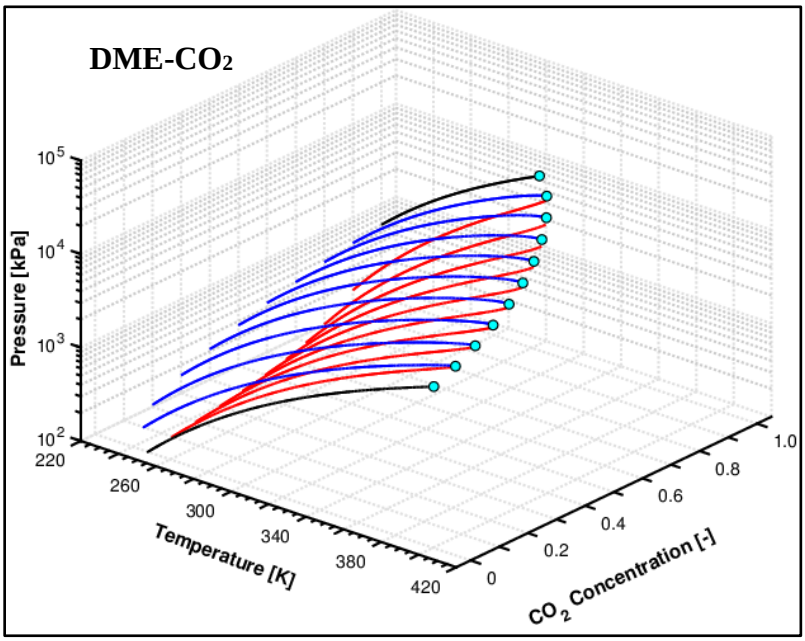

Figure 15. Phase envelope diagrams (3D) for DME-CO_2 zeotropic mixture at varying CO_2 concentrations

The pure HCs considered in the previous section, i.e., DME, R1234yf, DEE, and isobutane, are highly flammable (except for R1234yf, which has low flammability) according to the ASHRAE safety classification [19]. Due to their high flammability, they often face restrictions for use as WFs. A potential solution to this problem is to form the

zeotropic mixtures of these HCs with CO_2, which reduces WF flammability, making their use in the system more acceptable.

The SORC system using zeotropic mixtures (shown in Figure 3) is considered in this study. The performance of the system is analyzed for the four zeotropic mixtures, namely DME-CO_2, R1234yf-CO_2, DEE-CO_2, and isobutane-CO_2, at different heat-source inlet temperatures (T_5) with variations in evaporator pressure (P_2) above the critical pressure (P_c). The reduced pressure (θ) is varied from one to four, while the heat-source inlet temperature is varied from 400 K to 500 K. The thermophysical properties of the WFs are computed using the REFPROP 9.1, which is combined with PYTHON through an interface. The zeotropic mixtures in this study are formed on a molar concentration basis. The fractional molar concentration (σ), defined as the ratio of the number of moles of HC and the total number of moles in the mixture, is varied from 0.2 to 0.8 (20% to 80% HC). A higher value of σ indicates a higher HC concentration in the mixture. The cycle's performance is analyzed based on cycle efficiency, VPC, exergy efficiency, and non-dimensional exergy destruction.

4.1. Cycle Efficiency

Figures 16, 18, and 19 show the impact on the cycle efficiency of varying reduced pressure (θ) at different heat-source inlet temperatures (T_5) and fractional molar concentrations (σ) for all the WFs. In general, these figures show that the cycle efficiency for the WFs initially increases with reduced pressure and then decreases at higher values of θ. The same trend is observed at each heat-source inlet temperature and fractional molar concentration.

Figures 16 shows the impact on the cycle efficiency (η) of varying reduced pressure (θ) at a heat-source inlet temperature (T_5) of 400 K for different fractional molar concentrations (σ) for all the WFs. Figure 16 generally shows better cycle performance for DME-CO_2 zeotropic mixture compared to other WFs at lower values of θ, such as σ = 0.2, 0.4, and 0.6. The DEE-CO_2 zeotropic mixture demonstrates a cycle efficiency better than that of other WFs for higher values of θ for the same σ. For σ = 0.8, the DME-CO_2 zeotropic mixture shows a better cycle efficiency compared to other WFs at the critical point (θ = 1), whereas the R1234yf-CO_2 shows a better cycle efficiency than the other WFs for θ values greater than 1. The figure also shows that with an increase in the HC concentration (i.e., with an increase in σ), the cycle efficiency increases with an increase in θ for the WFs. However, with an increase in σ, the maximum cycle efficiency for the WFs moves to the subcritical region. At a heat-source inlet temperature of 400 K, the DME-CO_2 zeotropic mixture demonstrates the maximum cycle efficiency of 7.68% at a reduced pressure of θ = 1 (6522 kPa) and σ = 0.8.

Figure 16 also shows a sudden increase in the cycle efficiency (3.87% to 4.2%) at σ = 0.2 and θ = 2.23 for the DEE-CO_2 zeotropic mixture. This increase in cycle efficiency is due to a considerable decrease in the mass flow rate of the WF at this point, which is the result of maintaining constant power output in the turbine. The mass flow rate of the WF depends on the work output from the turbine ($\dot{W}_t$) and the enthalpy difference between points 3 and 4 (Figure 3), according to Equation 10. As $\dot{W}_t$ is kept constant in this study, the decrease in the mass flow rate of the WF occurred due to the decrease in enthalpy at point 4, which is attributed to an unexpected change in temperature of point 4 (T_4). This

sudden temperature change at the turbine exit (T_4) is possibly the result of condensation within the turbine at this operating condition. The turbine operation needs to be studied at the same operating conditions to fully understand the effects of this temperature change. A similar trend can be observed for the DEE-CO_2 zeotropic mixture at $\sigma = 0.4$ and $\theta = 1.5$.

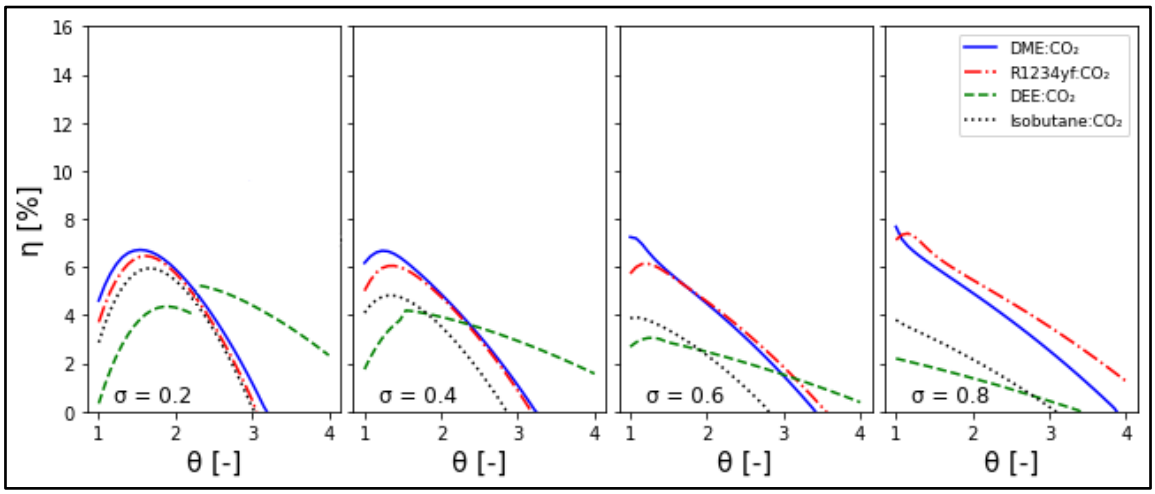

Figure 16. Cycle efficiency (η) variation with reduced pressure (θ) for different fractional molar compositions (σ) at heat-source inlet temperature of 400 K

Another important observation in Figure 16 is that the cycle efficiency can reach zero at higher values of θ for different fractional molar concentrations. This decreasing to zero is associated with the pump work ($\dot{W}p$) increasing to the point of exceeding the turbine work ($\dot{W}_t$) at higher values of θ as shown in Figure 17.

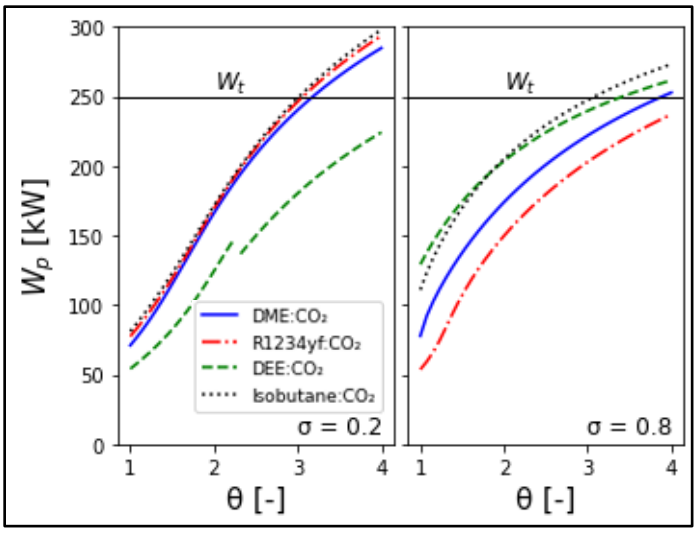

Figure 17. Pump Work ($\dot{W}_p$) variation with reduced pressure (θ) for different fractional molar compositions (σ) at heat-source inlet temperature of 400 K

Figures 18 shows the impact on the cycle efficiency (η) of varying reduced pressure (θ) at a heat-source inlet temperature (T_5) of 450 K for different fractional molar concentrations (σ) for all the WFs. Figure 18 generally shows a cycle efficiency that is better for a DME-CO_2 zeotropic mixture compared to other WFs for all values of θ at σ = 0.2, 0.4, and 0.6. For σ = 0.8, the DME-CO_2 zeotropic mixture demonstrates a better cycle efficiency compared to other WFs for θ values lower than 2.62, whereas the R1234yf-CO_2 zeotropic mixture shows a better cycle efficiency than other WFs for θ values greater than 2.62. At a heat-source inlet temperature of 450 K, the DME-CO_2 zeotropic mixture demonstrates the maximum cycle efficiency of 12.1% at θ = 1.38 (9000 kPa) and σ = 0.8. A similar trend can be observed for the DEE-CO_2 zeotropic mixture at σ = 0.4 and θ = 2.37.

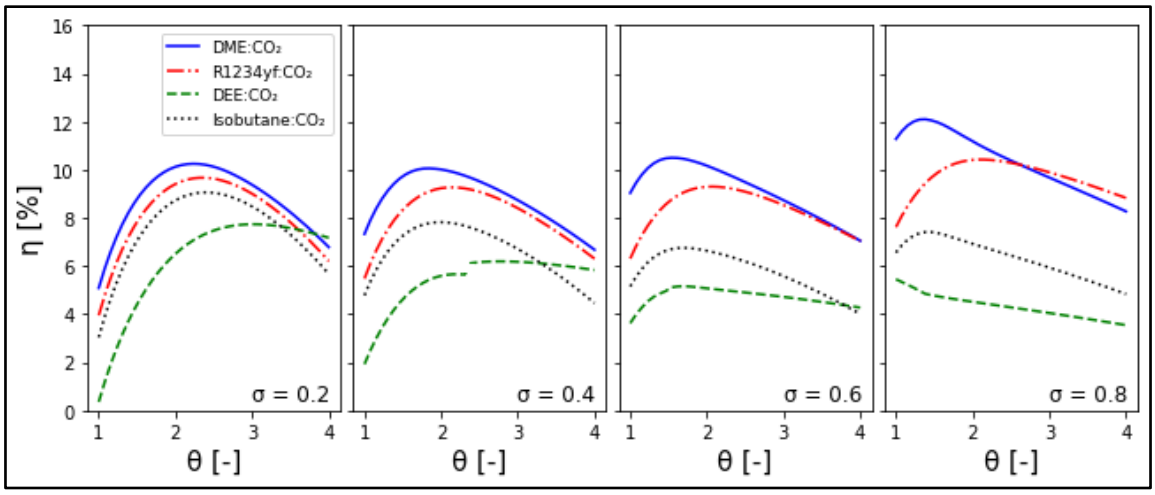

Figure 18. Cycle efficiency (η) variation with reduced pressure (θ) for different fractional molar compositions (σ) at heat-source inlet temperature of 450 K

Figures 19 shows the impact on cycle efficiency (η) of varying reduced pressure (θ) at a heat-source inlet temperature (T_5) of 450 K for different fractional molar concentrations (σ) for all the WFs. As expected, this figure generally shows better cycle efficiency for the DME-CO_2 zeotropic mixture compared to other WFs for all values of θ and σ. At a heat-source inlet temperature of 500 K, the DME-CO_2 zeotropic mixture demonstrates the maximum cycle efficiency of 15% at θ = 2.24 (14604 kPa) and σ = 0.8.

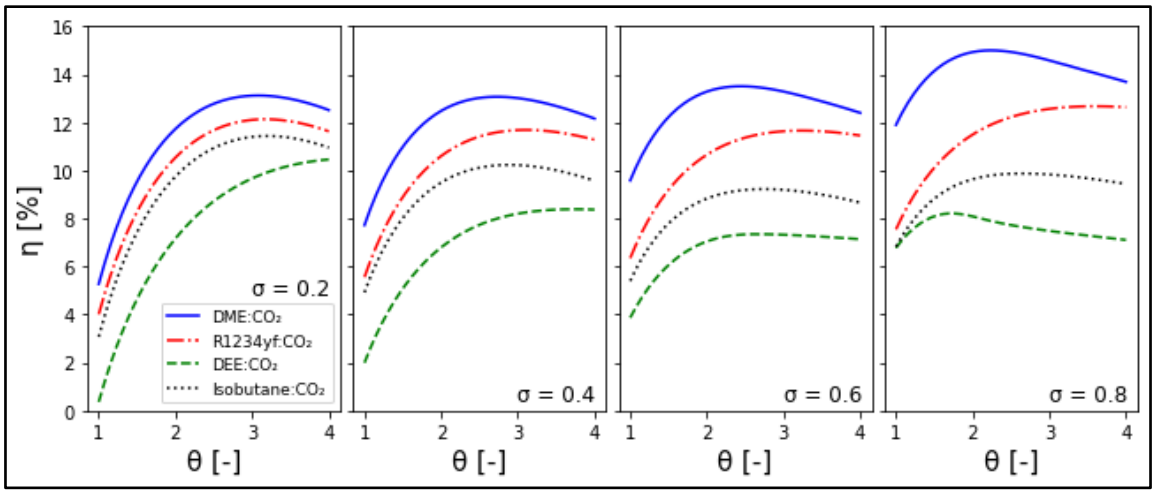

Figure 19. Cycle efficiency (η) variation with reduced pressure (θ) for different fractional molar compositions (σ) at heat-source inlet temperature of 500 K

A vital observation drawn from Figures 16, 18, and 19 is that the cycle efficiency (η) increases with increased heat-source inlet temperature (T_5). Another vital observation drawn from these figures is that the DME-CO_2 zeotropic mixture is suitable for the system because of its superior cycle performance when the heat-source inlet temperature varies from 400 K to 500 K, and the fractional molar concentration varies from 0.2 to 0.8. On comparing the results of cycle efficiency of the HC-CO_2 zeotropic mixtures (Figures 16, 18, and 19) and the pure HCs (Figure 6), the results show that the cycle efficiency of pure HCs is higher than the cycle efficiency of HC-CO_2 zeotropic mixtures, as an example, a difference of 2.9% exists between the maximum cycle efficiencies obtained at 500 K.

4.2. Volumetric Power Coefficient

VPC, as mentioned in the previous section, may be used to interpret the size of the system in terms of work output for different WFs [10]. A higher value of VPC is desirable for the WF, as it indicates that the system produces the same power output with less

volume flow of the WF at the turbine's inlet. Figures 20, 21, and 22 show the impact on the VPC of varying reduced pressure (θ) at different heat-source inlet temperatures (T_5) and fractional molar concentrations (σ) for all the WFs. The trends obtained in Figures 20, 21, and 22 show that the VPC increases with a rise in reduced pressure for all heat-source inlet temperatures and fractional molar concentrations.

The results obtained from Figures 20, 21, and 22 indicate the superiority of the DME-CO_2 zeotropic mixture in system sizing followed by the R1234yf-CO_2 zeotropic mixture when the heat-source inlet temperature varies from 400 K to 500 K, and fractional molar concentration varies from 0.2 to 0.8. For all heat-source inlet temperatures, the DEE-CO_2 zeotropic mixture has a low VPC of 0.15 MJ/m^3 at 5612 kPa (critical point, θ = 1) and σ = 0.2, which is due to the higher specific volume at the inlet of the turbine (v_{in}), as a result of lower value of density at this point.

Comparing the VPCs of the HC-CO_2 zeotropic mixtures (Figures 20, 21, and 22) and the pure HCs (Figure 8), the results show that the HC-CO_2 zeotropic mixtures have better VPC characteristics than the pure HCs for all heat-source inlet temperatures (T_5).

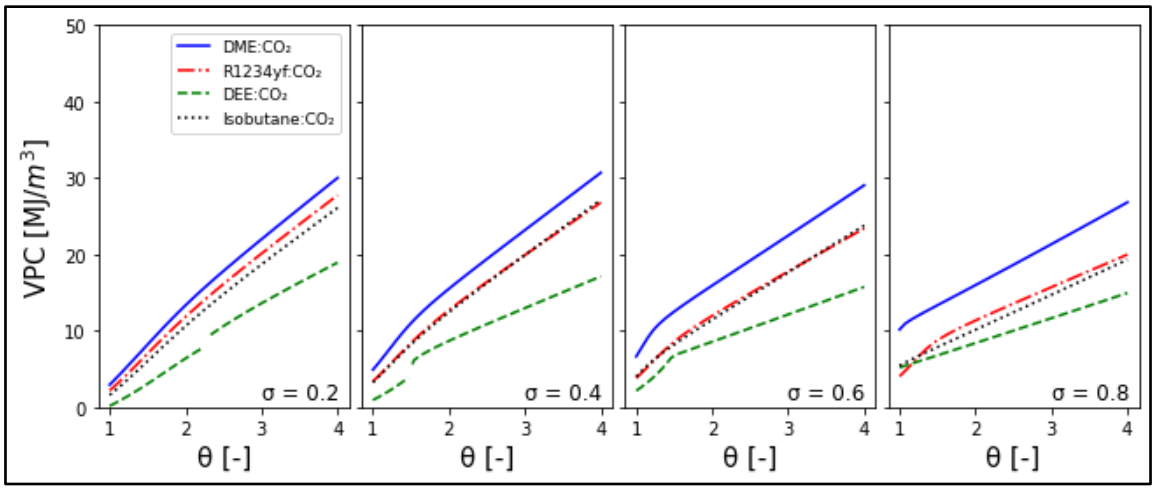

Figure 20. Volumetric power coefficient (*VPC*) variation with reduced pressure (θ) for different fractional molar compositions (σ) at heat-source inlet temperature of 400 K

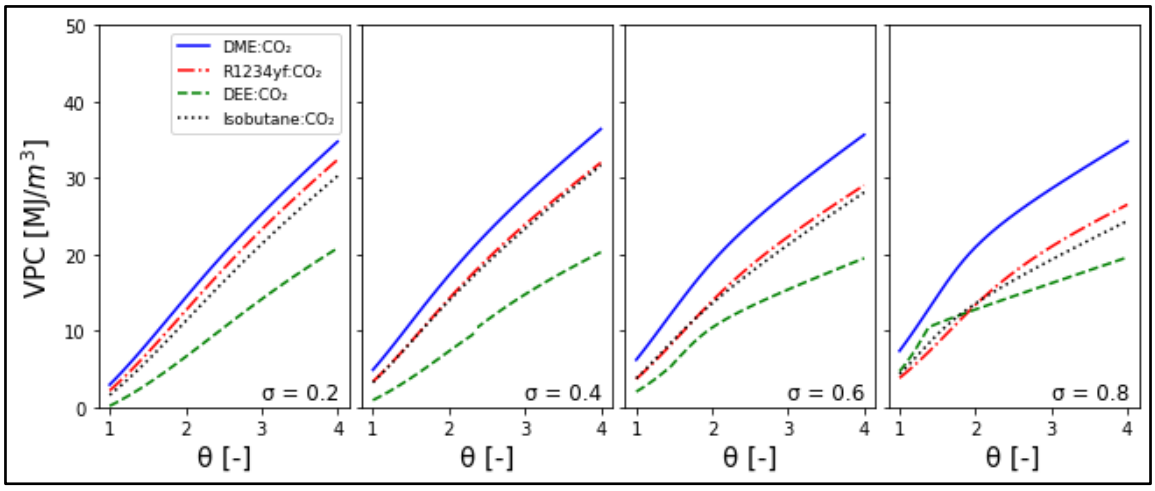

Figure 21. Volumetric power coefficient (*VPC*) variation with reduced pressure (θ) for different fractional molar compositions (σ) at heat-source inlet temperature of 450 K

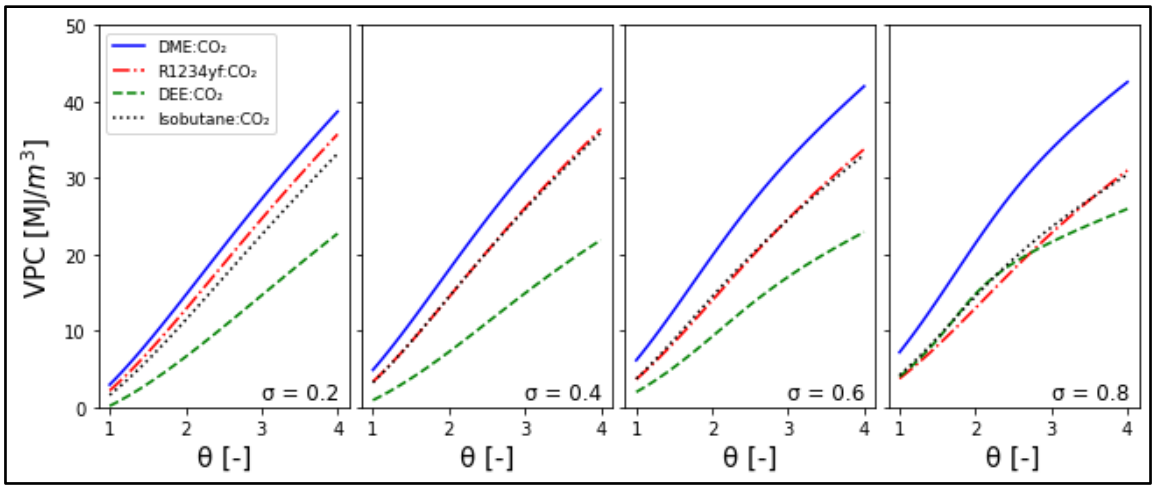

Figure 22. Volumetric power coefficient (*VPC*) variation with reduced pressure (θ) for different fractional molar compositions (σ) at heat-source inlet temperature of 500 K

4.3. Exergy Efficiency

The exergy efficiency of the system (also known as second law efficiency) is defined as the ratio of net work output of the cycle and exergy input to the cycle from a low-grade heat source. A higher value of exergy efficiency is desirable for the system as it indicates that the available energy from the low-grade heat source is utilized efficiently. If the net work output for the system is fixed, a higher value of η_s will indicate lower total exergy destruction and higher cycle efficiency, which will lower the cost of the system. The exergy efficiency (η_s) for the SORC system is computed using Equation 12 for the four zeotropic mixtures considered in this study. Figures 23, 24, and 25 show the impact on the exergy efficiency (η_s) of varying reduced pressure (θ) at different heat-source inlet temperatures (T_5) and fractional molar concentrations (σ) for all the WFs.

Figure 23 generally shows a cycle performance in terms of exergy efficiency for the DME-CO_2 zeotropic mixture that is better than the other WFs at lower values of θ at

σ = 0.2, 0.4, and 0.6. Additionally, the DEE-CO_2 zeotropic mixture demonstrates a better exergy efficiency than the other WFs at higher values of θ for the same σ. For σ = 0.8, the DME-CO_2 zeotropic mixture shows a better exergy efficiency than the other WFs at the critical point (θ = 1), whereas the R1234yf-CO_2 zeotropic mixture shows better exergy efficiency than other WFs for θ values greater than 1. The figure also shows that with an increase in the HC concentration (i.e., with an increase in σ), the exergy efficiency for the WFs increases with an increase in θ. However, with an increase in σ, the maximum exergy efficiency for the WFs moves to the subcritical region.

At a heat-source inlet temperature of 400 K, the DME-CO_2 zeotropic mixture demonstrates the maximum exergy efficiency of 33.26% at θ = 1 (6522 kPa) and σ = 0.8. Similar to Figure 16, at σ = 0.2 and θ = 2.23, there is a sudden increase in the exergy efficiency (16.77% to 18.2%) for the DEE-CO_2 zeotropic mixture. As explained before in Figure 16, the sudden increase in exergy efficiency for the DEE-CO_2 zeotropic mixture is attributed to the decrease in enthalpy of the WF at point 4, which is caused by an abrupt change in temperature at point 4. The same trend is observed for the DEE-CO_2 zeotropic mixture at σ = 0.4 and θ = 1.5.

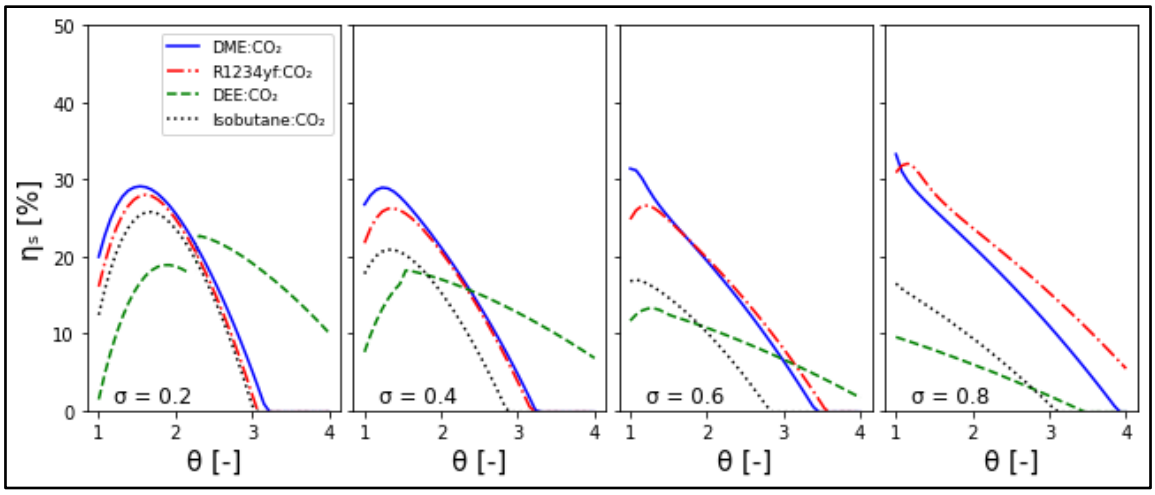

Figure 23. Exergy efficiency (η_s) variation with reduced pressure (θ) for different fractional molar compositions (σ) at heat-source inlet temperature of 400 K

Figure 24 generally shows a cycle performance in terms of exergy efficiency for the DME-CO_2 zeotropic mixture that is better than the other WFs for all values of θ at σ = 0.2, 0.4, and 0.6. For σ = 0.8, the DME-CO_2 zeotropic mixture demonstrates better exergy efficiency than other WFs for θ values lower than 2.62, whereas the R1234yf-CO_2 zeotropic mixture shows better exergy efficiency than other WFs for θ values greater than 2.62. At a heat-source inlet temperature of 450 K, the DME-CO_2 zeotropic mixture demonstrates the maximum exergy efficiency of 38.04% at θ = 1.38 (9000 kPa) and σ = 0.8. A similar trend (observed in Figure 23 for σ = 0.2 and 0.4) is also observed for the DEE-CO_2 zeotropic mixture at σ = 0.4 and θ = 2.37 due to similar reason.

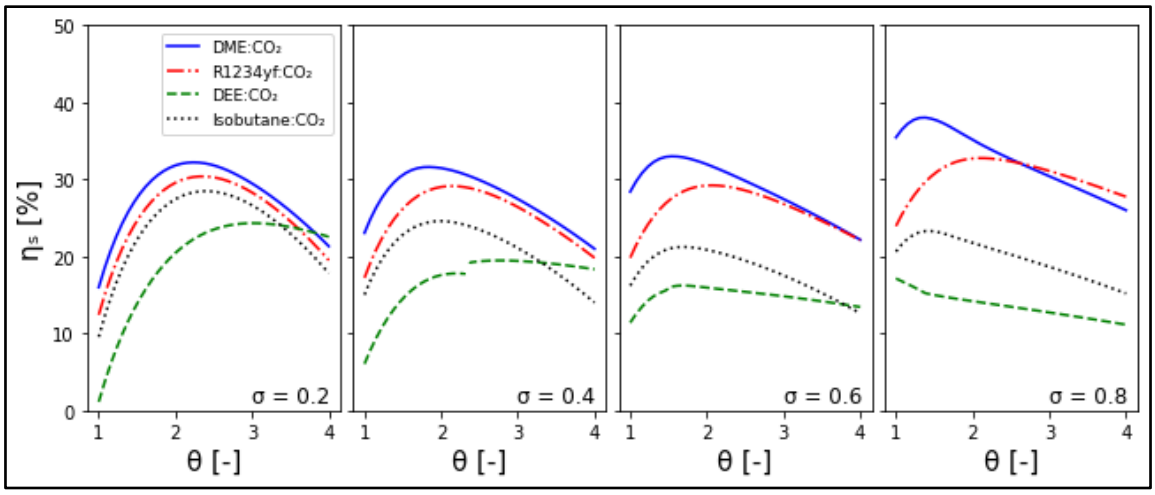

Figure 24. Exergy efficiency (η_s) variation with reduced pressure (θ) for different fractional molar compositions (σ) at heat-source inlet temperature of 450 K

Figure 25 generally shows a cycle performance in terms of exergy efficiency for the DME-CO_2 zeotropic mixture that is better than the other WFs for all values of θ and σ. At a heat-source inlet temperature of 500 K, the DME-CO_2 zeotropic mixture demonstrates the maximum exergy efficiency of 38.68% at θ = 2.24 (14604 kPa) and σ = 0.8. A vital observation drawn from Figures 23, 24, and 25 is that the exergy efficiency (η) increases with increased heat-source inlet temperature (T_5). Another vital observation drawn from Figures 23, 24, and 25 is that the DME-CO_2 zeotropic mixture is a suitable WF for the system due to its superior exergy performance as the heat-source inlet temperature varies from 400 K to 500 K, and fractional molar concentration varies from 0.2 to 0.8.

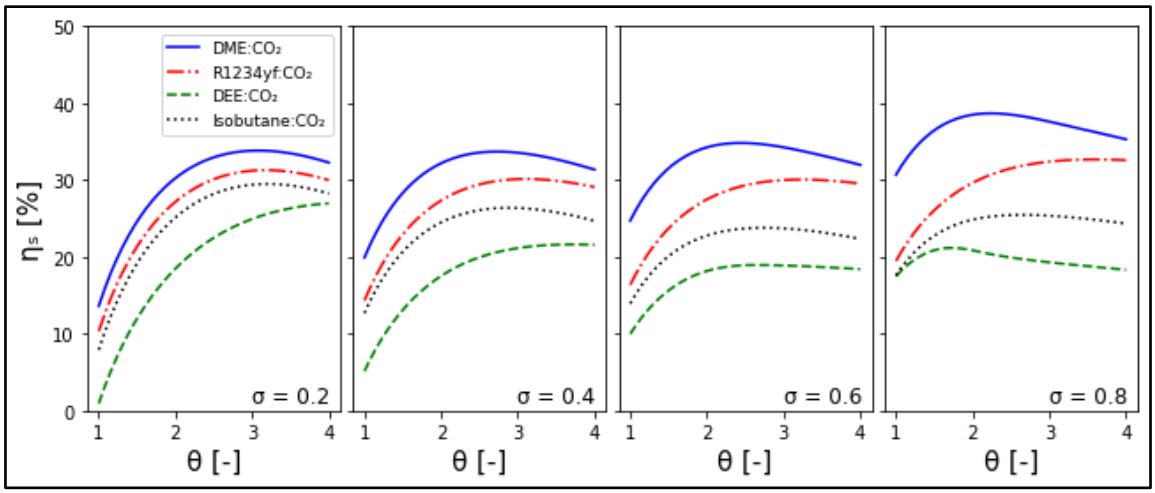

Figure 25. Exergy efficiency (η_s) variation with reduced pressure (θ) for different fractional molar compositions (σ) at heat-source inlet temperature of 500 K

4.4. Non-Dimensional Exergy Destruction

The total non-dimensional exergy destruction of the system (λ_{Total}) is defined as the ratio of the system's total exergy destruction and the exergy input to the cycle from the low-grade heat source. The lower value of λ_{Total} indicates efficient utilization of the energy available in the low-grade heat source, resulting in cost-effective systems. The total exergy destruction ($\dot{X}D_{Total}$) in the SORC system was calculated for all the zeotropic mixtures considered in this study, using Equation 17, at different heat-source inlet temperatures (T_5) and reduced pressures (θ). The total non-dimensional exergy destruction (λ_{Total}) in the SORC system was then calculated using Equation 19. The results were plotted as a function of reduced pressure as the heat-source inlet temperature is varied from 400 K to 500 K, and fractional molar concentration (σ) is varied from 0.2 to 0.8. The results are shown in Figures 26, 27, and 28.

The results clearly show that the DME-CO_2 zeotropic mixture has the lowest total non-dimensional exergy destruction for the system for all heat-source inlet temperatures and fractional molar concentrations compared to other WFs. On the other hand, the DEE-CO_2 zeotropic mixture shows the highest total non-dimensional exergy destruction compared to the other WFs, followed by the isobutane-CO_2 zeotropic mixture. The contents of Figures 26, 27, and 28 verify the previous results for the exergy efficiency (shown in Figures 23, 24, and 25), in that, the DME-CO_2 zeotropic mixture shows clear superiority over other WFs that are considered in this study.

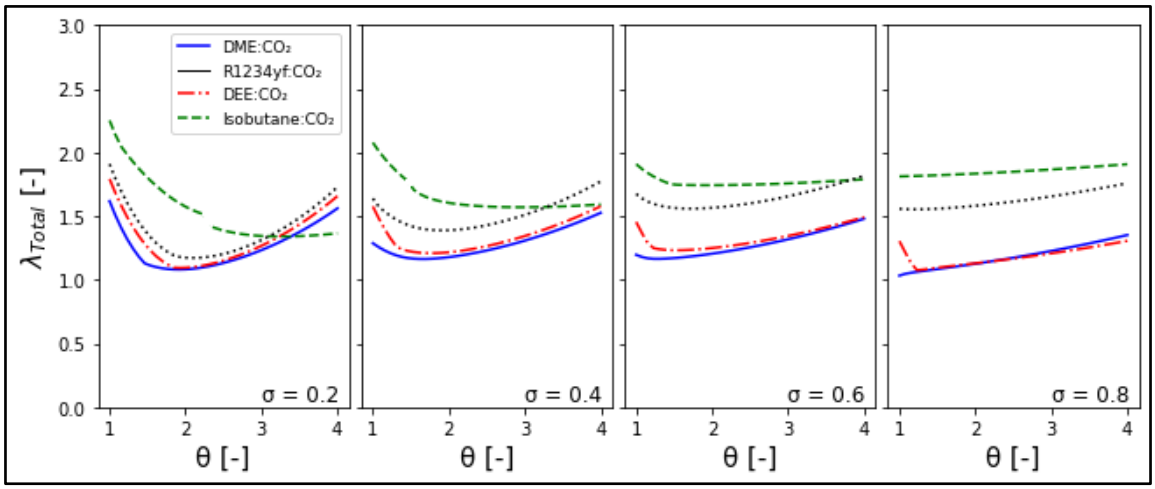

Figure 26. Variation of total non-dimensional exergy destruction (λ_{Total}) in the system with reduced pressure (θ) for different fractional molar compositions (σ) at heat-source inlet temperature of 400 K

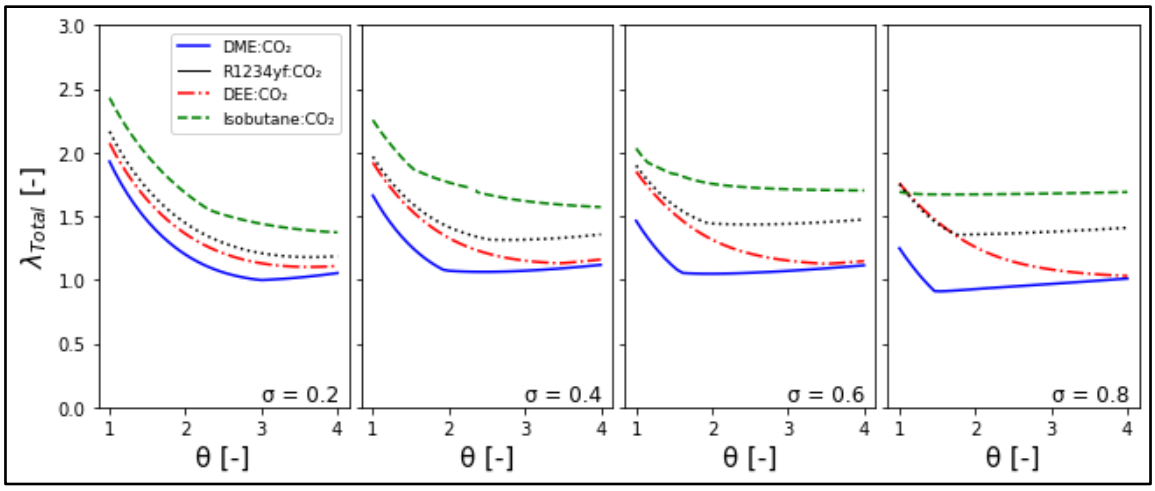

Figure 27. Variation of total non-dimensional exergy destruction (λ_{Total}) in the system with reduced pressure (θ) for different fractional molar compositions (σ) at heat-source inlet temperature of 450 K

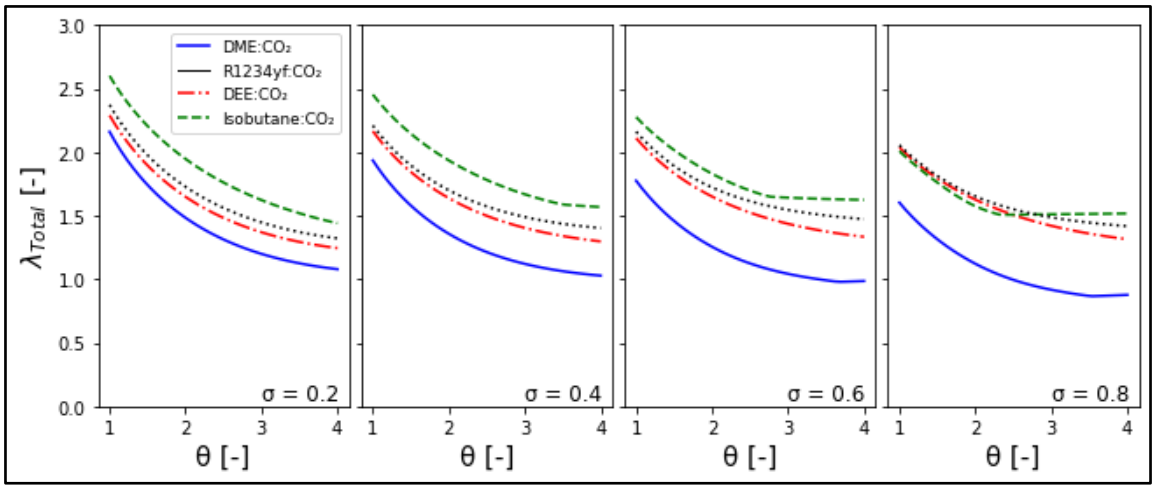

Figure 28. Variation of total non-dimensional exergy destruction (λ_{Total}) in the system with reduced pressure (θ) for different fractional molar compositions (σ) at heat-source inlet temperature of 500 K

Therefore, based on the energy and exergy analysis, the DME-CO_2 zeotropic mixture is the most suitable WF for SORC for those operating conditions considered in this study. Although the cycle efficiency of the zeotropic mixtures considered in this study

is lower than the pure HCs, they are more environmentally friendly than pure HCs because of lower flammability.

5. APPLICATION

In the previous studies, a comprehensive analysis was conducted to evaluate the performance of different pure organic fluids and zeotropic mixtures as WFs for the SORC system to identify the optimal WFs for the operating conditions considered. However, the main objective of this study was to assess the performance of the optimal zeotropic mixture as a WF for the SORC system located in a Houston-based facility. The performance is evaluated for the summer and winter temperatures of 5°C (278 K) and 35°C (308 K). Table 5 shows the maximum and minimum monthly temperature in °C for the city of Houston. The temperatures selected from this data will be used to reference the dead state and heat-sink temperatures.

Table 5. Average monthly and annual temperature of Houston in °C [38]

	Jan	**Feb**	**Mar**	**Apr**	**May**	**Jun**	**Jul**	**Aug**	**Sep**	**Oct**	**Nov**	**Dec**
Max	17.7	19.9	23.3	26.7	30.5	33.5	34.7	34.9	32.4	28.2	22.6	18.5
Min	6.5	8.7	12.0	15.4	19.9	23.2	24.3	24.1	21.4	16.1	10.8	7.6

The performance of the system is analyzed for the DME-CO_2 zeotropic mixture, which was selected as the optimal WF in the previous chapter, at different heat-source inlet temperatures (T_5) and heat-sink temperature (T_7) along with variations in evaporator pressure (P_2) above the critical pressure (P_c) of the WF. The reduced pressure (θ) is varied from one to four, while the heat-source inlet temperature is varied from 400 K to 500 K. The thermophysical properties of the WF are computed using REFPROP 9.1, which is

combined with PYTHON through an interface. The zeotropic mixture in this study is formed on a molar concentration basis. The fractional molar concentration (σ) is varied from 0.2 to 0.8 (20% to 80% HC). A higher value of σ indicates a higher HC concentration in the mixture. The heat-sink temperatures (T_7) used in this study are 278 K and 308 K. The results for the performance of the WF in terms of cycle efficiency, VPC, exergy efficiency, and exergy destruction will provide information about whether this WF is suitable for the location (i.e., Houston) considered. This study provides a framework for selecting WFs for different locations in the United States and worldwide.

5.1. Cycle Efficiency

Figures 29, 30, and 31 show the impacts of variations in reduced pressure (θ) on the cycle efficiency (η) of the DME-CO_2 zeotropic mixture at different heat-source inlet temperatures (T_5) for different heat-sink temperatures (T_7) and fractional molar concentrations (σ). In general, these figures show that the cycle efficiency for the DME-CO_2 zeotropic mixture for both heat-sink temperatures (T_7) initially increases with an increase in reduced pressure (θ), and then decreases for higher values of θ. The same trend is obtained at each heat-source inlet temperature and fractional molar concentration. The figures indicate that the DME-CO_2 zeotropic mixture has a better cycle performance at a lower value of heat-sink temperature, i.e., at T_7 = 278 K. The figures also show that the cycle efficiency for the mixture increases with an increase in heat-source inlet temperature (T_5).

At a heat-source inlet temperature of 400 K, the maximum cycle efficiency for the DME-CO_2 zeotropic mixture at T_7 = 278 K is 10.43% at θ = 1 (6522 kPa) and σ = 0.8,

whereas the maximum cycle efficiency at T_7 = 308 K is 6.70% at θ = 1 (6522 kPa) and σ = 0.8. At 450 K, the maximum cycle efficiency for DME-CO_2 zeotropic mixture at T_7 = 278 K is 14.94% at θ = 1.31 (8544 kPa) and σ = 0.8, whereas the maximum cycle efficiency at T_7 = 308 K is 11.11% at θ = 1.38 (9000 kPa) and σ = 0.8. At 500 K, the maximum cycle efficiency for DME-CO_2 zeotropic mixture at T_7 = 278 K is 17.72% at θ = 2.12 (13827 kPa) and σ = 0.8, whereas the maximum cycle efficiency at T_7 = 308 K is 14.04% at θ = 2.27 (14805 kPa) and σ = 0.8. The figures also show that with an increase in the HC concentration (i.e., with an increase in σ), the cycle efficiency for the DME-CO_2 zeotropic mixture, for both heat-sink temperatures, increases with an increase in θ. However, with an increase in σ, the maximum cycle efficiency for the mixture moves to the subcritical region.

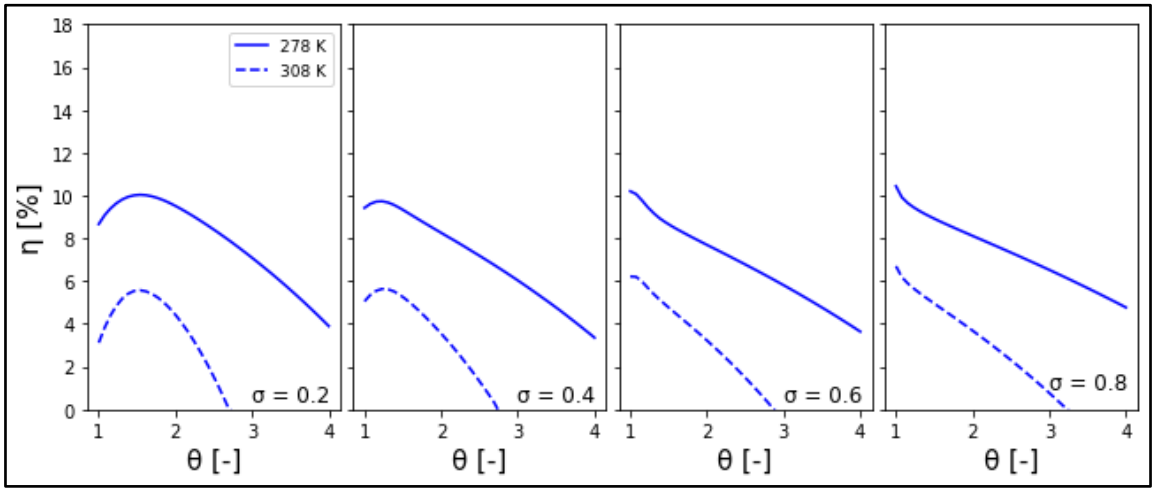

Figure 29. Cycle efficiency (η) variation for DME-CO_2 zeotropic mixture with reduced pressure (θ) for different fractional molar compositions (σ) and heat-sink temperatures (T_7) at heat-source inlet temperature of 400 K

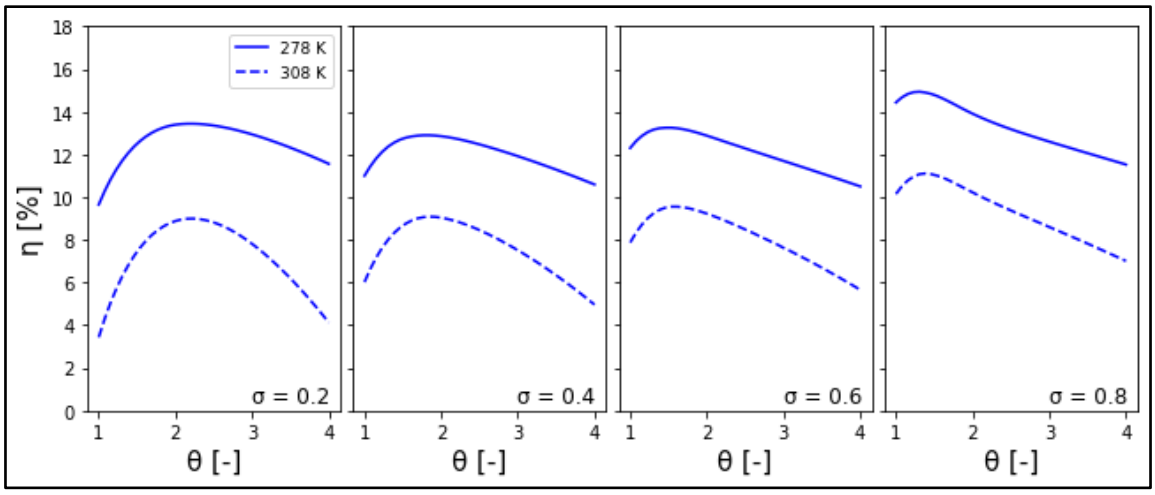

Figure 30. Cycle efficiency (η) variation for DME-CO_2 zeotropic mixture with reduced pressure (θ) for different fractional molar compositions (σ) and heat-sink temperatures (T_7) at heat-source inlet temperature of 450 K

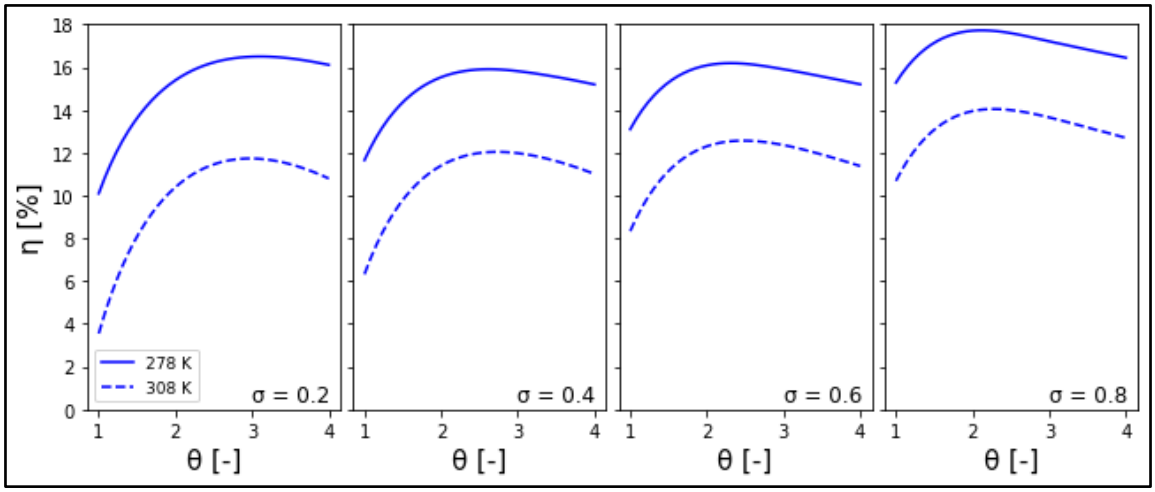

Figure 31. Cycle efficiency (η) variation for DME-CO_2 zeotropic mixture with reduced pressure (θ) for different fractional molar compositions (σ) and heat-sink temperatures (T_7) at heat-source inlet temperature of 500 K

5.2. Volumetric Power Coefficient

VPC, as mentioned in the previous section, may be used to interpret the size of the system in terms of work output for different WFs [10]. A higher value of VPC is desirable

for the WF, as it indicates that the system produces the same power output with less volume flow of the WF at the turbine inlet. Figures 32, 33, and 34 show the impact of variation of reduced pressure (θ) on the VPC of the DME-CO_2 zeotropic mixture at different heat-source inlet temperatures (T_5) for different heat-sink temperatures (T_7) and fractional molar concentrations (σ). The trends obtained for the mixture at both heat-sink temperatures (T_7) in Figures 32, 33, and 34 show that the VPC for the DME-CO_2 zeotropic mixture increases monotonically with reduced pressure for all heat-source inlet temperatures and fractional molar concentrations. The figures also indicate that the DME-CO_2 zeotropic mixture has better system sizing characteristics at a lower value of heat-sink temperature, i.e., at T_7 = 278 K.

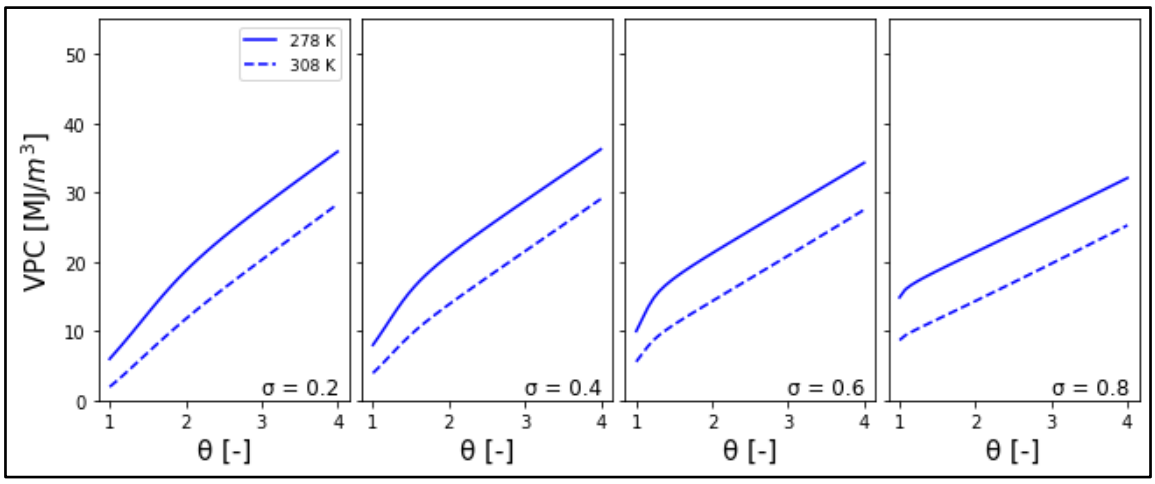

Figure 32. Volumetric power coefficient (*VPC*) variation for DME-CO_2 zeotropic mixture with reduced pressure (*θ*) for different fractional molar compositions (*σ*) and heat-sink temperatures (T_7) at heat-source inlet temperature of 400 K

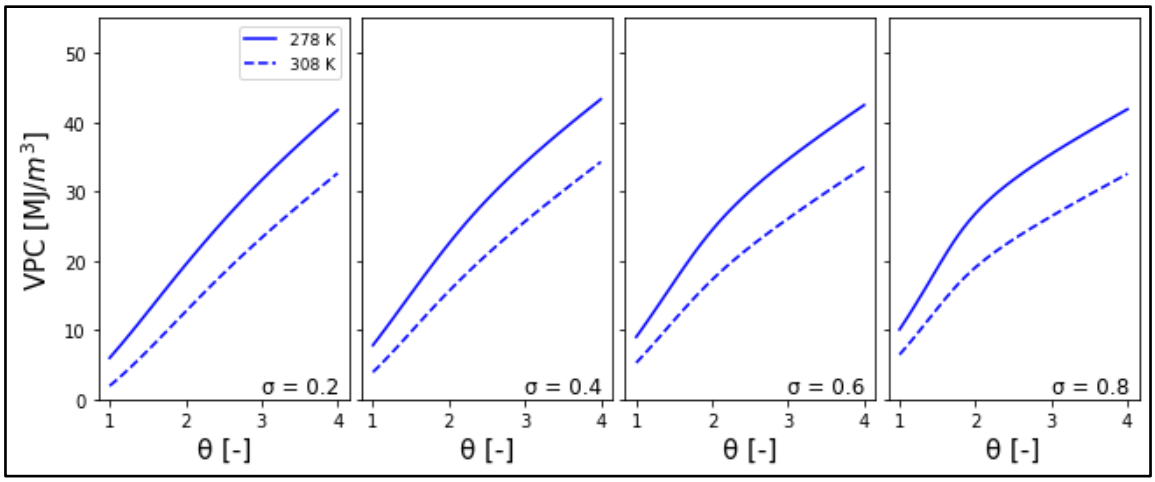

Figure 33. Volumetric power coefficient (*VPC*) variation for DME-CO_2 zeotropic mixture with reduced pressure (θ) for different fractional molar compositions (σ) and heat-sink temperatures (T_7) at heat-source inlet temperature of 450 K

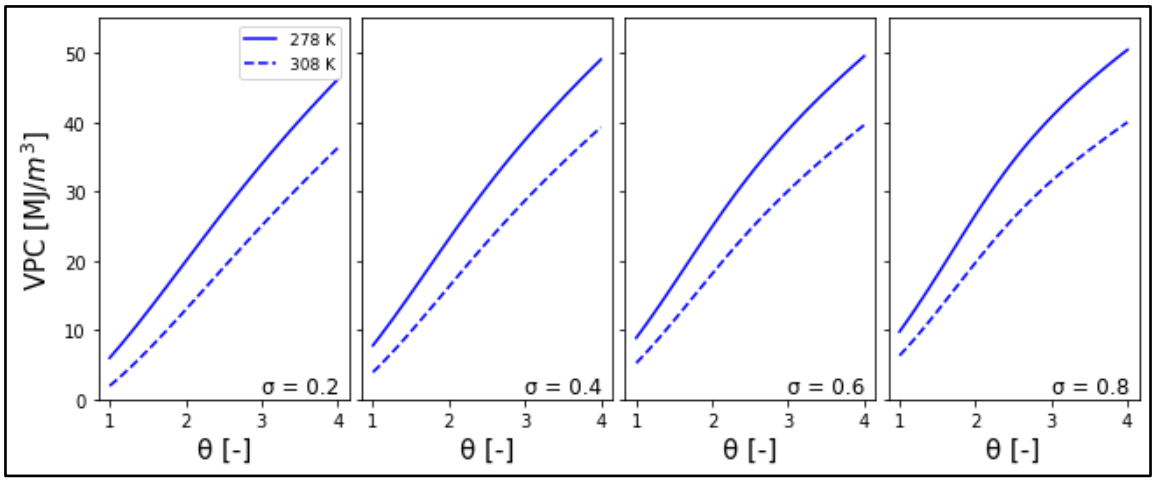

Figure 34. Volumetric power coefficient (*VPC*) variation for DME-CO_2 zeotropic mixture with reduced pressure (θ) for different fractional molar compositions (σ) and heat-sink temperatures (T_7) at heat-source inlet temperature of 500 K

5.3. Exergy Efficiency

The exergy efficiency (η_s), also known as second law efficiency, for the SORC system operating with the DME-CO_2 zeotropic mixture is computed using Equation 12. A

higher value of exergy efficiency is desirable for the system as it indicates that the available energy from the low-grade heat source is utilized efficiently. Figures 35, 36, and 37 show the impacts of reduced pressure (θ) variations on the exergy efficiency (η_s) of the DME-CO_2 zeotropic mixture for different heat-source inlet temperatures (T_5) at different heat-sink temperatures (T_7) and fractional molar concentrations (σ). The trends obtained in these figures are similar to the trends of cycle efficiency in Figures 29, 30, and 31. Specifically, the figures indicate that the DME-CO_2 zeotropic mixture has better exergy efficiency values at a lower value of heat-sink temperature, i.e., at T_7 = 278 K.

At a heat-source inlet temperature of 400 K, the maximum exergy efficiency for the DME-CO_2 zeotropic mixture at T_7 = 278 K is 36.34% at θ = 1 (6522 kPa) and σ = 0.8, whereas the maximum exergy efficiency at T_7 = 308 K is 31.87% at θ = 1 (6522 kPa) and σ = 0.8. At 450 K, the maximum exergy efficiency for DME-CO_2 zeotropic mixture at T_7 = 278 K is 40.57% at θ = 1.31 (8544 kPa) and σ = 0.8, whereas the maximum exergy efficiency at T_7 = 308 K is 37.03% at θ = 1.38 (9000 kPa) and σ = 0.8. At 500 K, the maximum exergy efficiency for DME-CO_2 zeotropic mixture at T_7 = 278 K is 40.96% at θ = 2.12 (13827 kPa) and σ = 0.8, whereas the maximum exergy efficiency at T_7 = 308 K is 37.80% at θ = 2.27 (14805 kPa) and σ = 0.8. The figures also show that with an increase in the HC concentration (i.e., with an increase in σ), the cycle efficiency for the DME-CO_2 zeotropic mixture, for both heat-sink temperatures, increases with an increase in θ. However, with an increase in σ, the maximum cycle efficiency for the mixture moves to the subcritical region.

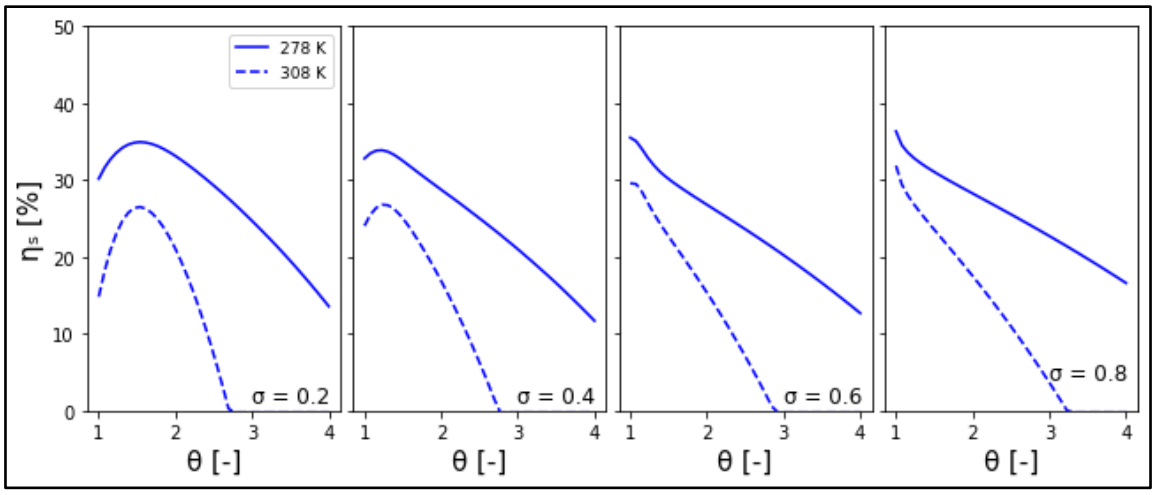

Figure 35. Exergy efficiency (η_s) variation for DME-CO_2 zeotropic mixture with reduced pressure (θ) for different fractional molar compositions (σ) and heat-sink temperatures (T_7) at heat-source inlet temperature of 400 K

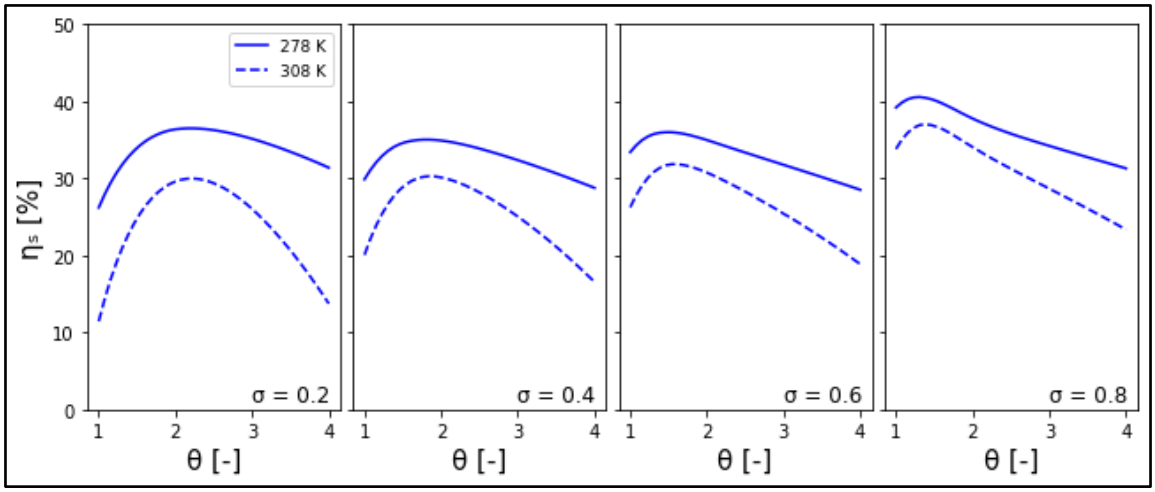

Figure 36. Exergy efficiency (η_s) variation for DME-CO_2 zeotropic mixture with reduced pressure (θ) for different fractional molar compositions (σ) and heat-sink temperatures (T_7) at heat-source inlet temperature of 450 K

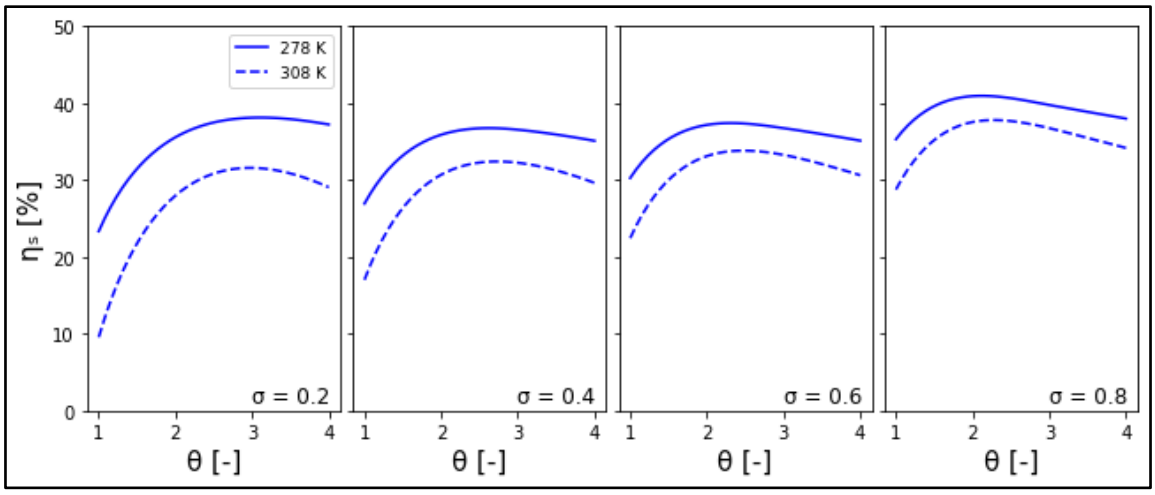

Figure 37. Exergy efficiency (η_s) variation for DME-CO_2 zeotropic mixture with reduced pressure (θ) for different fractional molar compositions (σ) and heat-sink temperatures (T_7) at heat-source inlet temperature of 500 K

5.4. Non-Dimensional Exergy Destruction

The total non-dimensional exergy destruction of the system (λ_{Total}) is defined as the ratio of the system's total exergy destruction and the exergy input to the cycle from the low-grade heat source. The lower value of λ_{Total} indicates efficient utilization of the energy available in the low-grade heat source, resulting in cost-effective systems. The total non-dimensional exergy destruction (λ_{Total}) in the SORC system operating with the DME-CO_2 zeotropic mixture was computed using Equation 19 for different heat-sink temperatures (T_7). The results were plotted as a function of reduced pressure (θ) when the heat-source inlet temperature (T_5) is varied from 400 K to 500 K, and the fractional molar concentration (σ) is varied from 0.2 to 0.8 as shown in Figures 38, 39, and 40.

The result clearly shows that the DME-CO_2 zeotropic mixture has the lowest total non-dimensional exergy destruction for the system at a lower value of the heat-sink temperature, i.e., at T_7 = 278 K. For the heat-source inlet temperatures of 400 K and 450

K, the DME-CO_2 zeotropic mixture, at both values of heat-sink temperature, initially decreases with an increase in reduced pressure and then increases for higher values of θ, as shown in Figures 38 and 39. In contrast, for a heat-source inlet temperature of 500 K, the DME-CO_2 zeotropic mixture exhibits a decreasing trend with increased reduced pressure, as shown in Figure 40. The highest value of λ_{Total} for the DME-CO_2 zeotropic mixture at T_5 = 400 K, for both values of heat-sink temperatures, is obtained at a reduced pressure value of 4 for all fractional molar concentrations. In comparison, the highest value of λ_{Total} for the DME-CO_2 zeotropic mixture at T_5 = 450 K and 500 K, for both values of heat-sink temperatures, is obtained at a reduced pressure value of 1 (i.e., critical point) for all fractional molar concentrations.

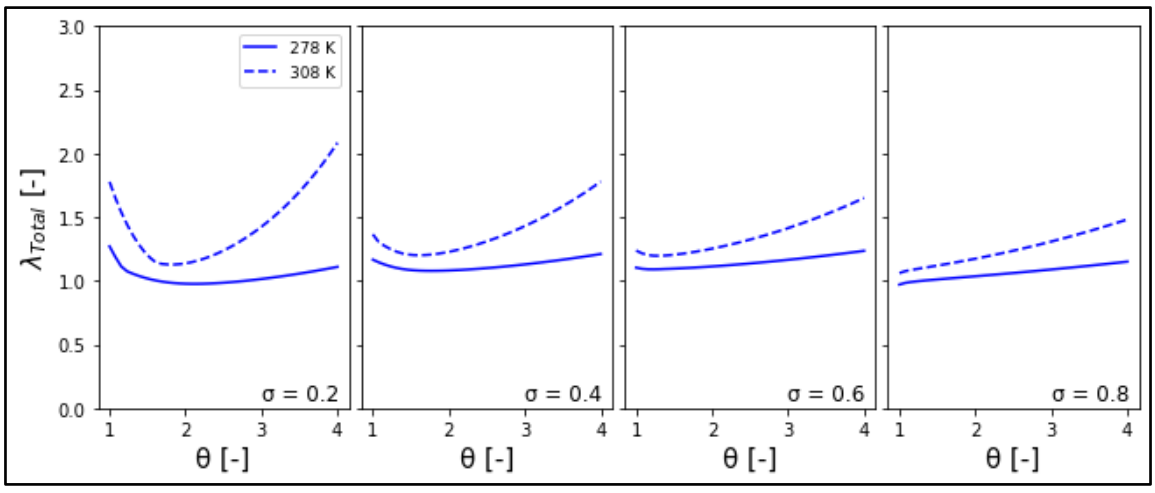

Figure 38. Variation of total non-dimensional exergy destruction (λ_{Total}) in the system for DME-CO_2 zeotropic mixture with reduced pressure (θ) for different fractional molar compositions (σ) and heat-sink temperatures (T_7) at heat-source inlet temperature of 400 K

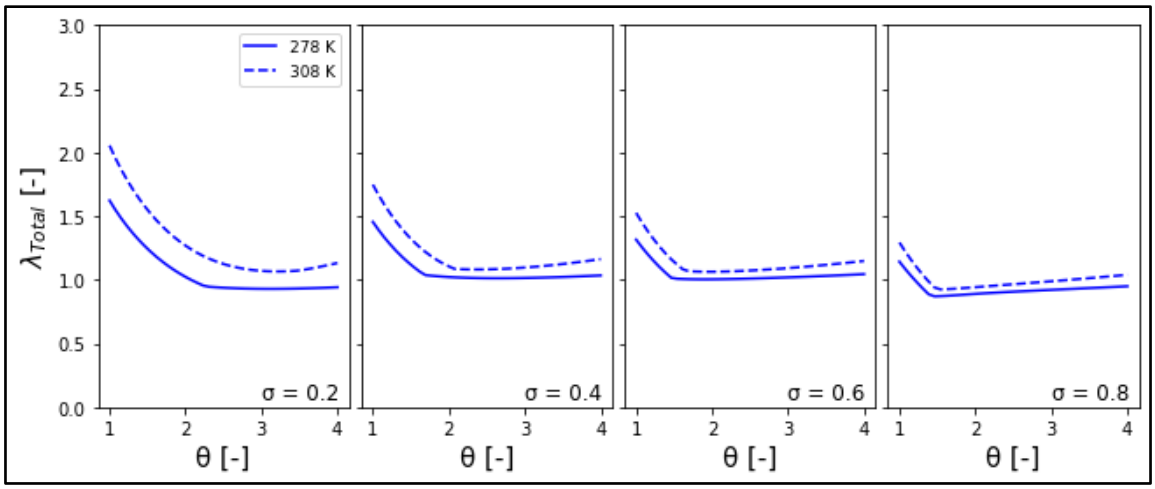

Figure 39. Variation of total non-dimensional exergy destruction (λ_{Total}) in the system for DME-CO_2 zeotropic mixture with reduced pressure (θ) for different fractional molar compositions (σ) and heat-sink temperatures (T_7) at heat-source inlet temperature of 450 K

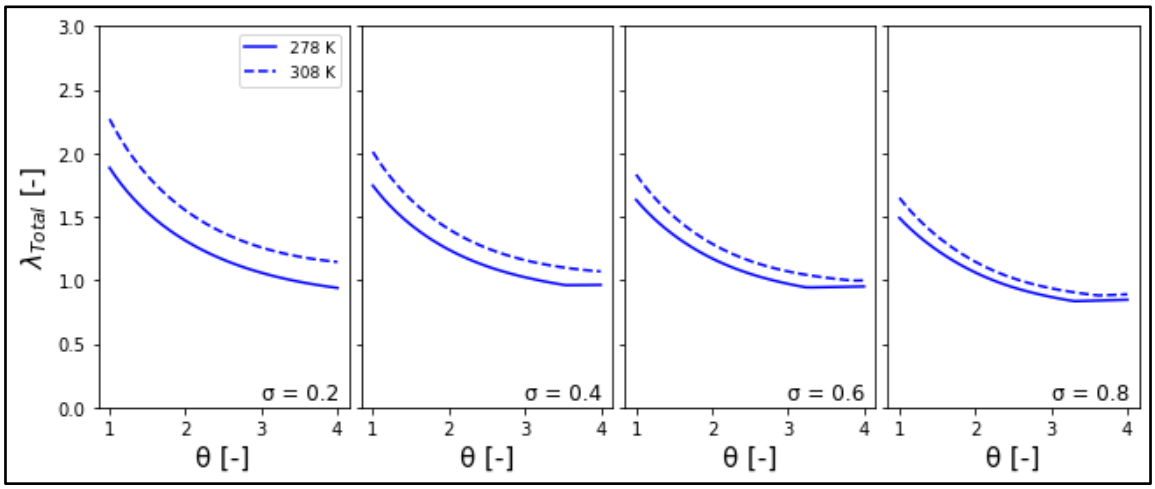

Figure 40. Variation of total non-dimensional exergy destruction (λ_{Total}) in the system for DME-CO_2 zeotropic mixture with reduced pressure (θ) for different fractional molar compositions (σ) and heat-sink temperatures (T_7) at heat-source inlet temperature of 500 K

6. CONCLUSIONS

In this study, four different HCs and their zeotropic mixtures (with CO_2) were investigated as potential WFs for a supercritical organic Rankine cycle (SORC) system. A low-grade waste heat source with inlet temperatures varying from 400 K to 500 K was considered as the hot source for the SORC system. The turbine work output for the system was kept constant at 250 kW. The zeotropic mixtures of the HCs and CO_2 were developed on a molar concentration basis, with the fractional molar concentration varying from 0.2 to 0.8 (20% to 80% HC). The computations conducted in the study were performed using several in-house PYTHON scripts. The thermophysical properties for the pure WFs were obtained using Engineering Equation Solver (EES), whereas REFPROP was used for the thermophysical properties of the zeotropic mixtures. The study identifies an environmentally friendly WF for the SORC system with low GWP, low flammability, low toxicity, and excellent thermodynamic performance for the experimental operating conditions. The optimal HC-CO_2 zeotropic blend was then used in a system located in a Houston-based facility, and its performance was assessed using the highest and lowest annual temperature of Houston (i.e., 308 K and 278 K) as the heat-sink and dead-state temperatures for the system.

The main conclusions from the study are summarized as follows,

- The energy analysis for both the pure fluids and the zeotropic mixtures shows that the cycle efficiency for the system increases with an increase in heat-source inlet temperature for all the WFs considered. For pure WFs, the energy analysis shows

that the maximum cycle efficiency of the system is obtained for different WFs at different heat-source inlet temperatures. In contrast, for zeotropic mixtures, the energy analysis shows that the maximum cycle efficiency of the system is obtained for the DME-CO_2 zeotropic mixture at a fractional molar concentration of 0.8 for all values of heat-source inlet temperature. The cycle efficiency of pure HCs is higher than the cycle efficiency of HC-CO_2 zeotropic mixtures, with a difference of 2.9% between the maximum cycle efficiencies obtained at 500 K.

- The VPC was computed for both pure WFs and zeotropic mixtures, and the results show that VPC increases with increases in the system pressure, which suggests that the system is more compact at higher heat-source inlet temperatures. The HC-CO_2 zeotropic mixtures have better VPC characteristics than the pure HCs for all heat-source inlet temperatures (T_5).
- The exergy analysis was conducted for both pure WFs and zeotropic mixtures. For pure WFs, the results show that the total exergy destruction in the system is highest for R1234yf and lowest for DME and DEE for all heat-source inlet temperatures. Whereas for zeotropic mixtures, the results show the total exergy destruction in the system is highest for the DEE-CO_2 zeotropic mixture followed by the isobutane-CO_2 zeotropic mixture. In contrast, the DME-CO_2 zeotropic mixture has the lowest total exergy destruction in the system and the highest exergy efficiency for all heat-source inlet temperatures and fractional molar concentration values.
- From the pure WFs, the DME was found to be the optimal WF for the system based on energy, exergy, exergoeconomic analyses, whereas from the zeotropic

mixtures, the DME-CO_2 zeotropic mixture was found to be the suitable WF for the system based on energy and exergy analyses. Although the cycle efficiency of the zeotropic mixtures considered in this study is lower than the pure HCs, they are safer to use than pure HCs because of lower flammability.

- The thermodynamic performance of the DME-CO_2 zeotropic mixture was then assessed for a system located in a Houston-based facility using Houston's highest and lowest annual temperatures as the heat-sink and dead-state temperatures for the system. The vital conclusion drawn from this analysis was that the DME-CO_2 zeotropic mixture performs better as the heat-sink temperature is decreased.

REFERENCES

[1] Waste Heat Recovery Resource Page (2017, January 2014). Retrieved from https://www.energy.gov/eere/amo/articles/waste-heat-recovery-resource-page [accessed on 02.06.2021]

[2] U.S. Energy Information Administration, "Manufacturing Energy Consumption Survey," (2014). Retrieved from https://www.eia.gov/consumption/manufacturing/data/2014/ [accessed on 09.29.2021]

[3] D. Vance, S. Nimbalkar, A. Thekdi, K. Armstrong, T. Wenning, J. Cresko, M. Jin, Estimation of and barriers to waste heat recovery from harsh environments in industrial processes, Journal of Cleaner Production, 2019, vol. 222, pp. 539-539. doi: 10.1016/j.jclepro.2019.03.011

[4] More power with Organic Rankine Cycle. Retrieved from https://www.e2singapore.gov.sg/DATA/0/docs/NewsFiles/More%20power%20with%20Organic%20Rankine%20Cycle_v3.pdf [accessed on 09.29.2021]

[5] Waste Heat Recovery: Technology and Opportunities in U.S. Industry. Retrieved from https://www1.eere.energy.gov/manufacturing/intensiveprocesses/pdfs/waste_heat_recovery.pdf [accessed on 02.07.2021]

[6] J. Sarkar, Review and future trends of supercritical CO2 Rankine cycle for low-grade heat conversion. Renewable and Sustainable Energy Reviews, 2015, vol. 48, pp. 434-451. doi:10.1016/j.rser.2015.04.039

[7] N. Zhou, X. Wang, Z. Chen, Z. Wang, Experimental Study on Organic Rankine Cycle for waste heat recovery from low-temperature flue gas, Energy, 2013, vol. 55, pp. 216-225. doi: 10.1016/j.energy.2013.03.047

[8] L. Xia, R. Liu, Y. Zeng, P. Zhou, J. Liu, X. Cao, S. Xiang, A review of low-temperature heat recovery technologies for industrial processes, Chinese Journal of Chemical Engineering, 2019, vol. 27, pp. 2227-2237. doi: 10.1016/j.cjche.2018.11.012

[9] C. Ji, Z. Qin, S. Dubey, F.H. Choo, F. Duan, Three-dimensional transient numerical study on latent heat thermal storage for waste heat recovery from a low temperature gas flow, Applied Energy, 2017, vol. 205, pp. 1-12. doi: 10.1016/j.apenergy.2017.07.101

[10] D. Das, M. Kazim, R. Sadr, M. Pate, Optimal hydrocarbon based working fluid selection for a simple supercritical Organic Rankine Cycle, Energy Conversion and Management, 2021, vol. 243. doi: 10.1016/j.enconman.2021.114424

[11] H. Gao, C. Liu, C. He, X. Xu, S. Wu, Y. Li, Performance Analysis and Working Fluid Selection of a Supercritical Organic Rankine Cycle for Low Grade Waste Heat Recovery, Energies, 2012, vol. 5, pp. 3233-3247. doi: 10.3390/en5093233

[12] H. Chen, D.Y. Goswami, M.M. Rahman, E.K. Stefanakos, A supercritical Rankine cycle using zeotropic mixture working fluids for the conversion of low-grade heat into power, Energy, 2011, vol. 36, pp. 549-555. doi: 10.1016/j.energy.2010.10.006

[13] S.C. Yelishala, K. Kannaiyan, R. Sadr, Z. Wang, Y.A. Levendis, H. Metghalchi, Performance maximization by temperature glide matching in energy exchangers of cooling systems operating with natural hydrocarbons/CO_2 refrigerants, International Journal of Refrigeration, 2020, vol. 110, pp. 294-304. doi: 10.1016/j.ijrefrig.2020.08.006

[14] S.C. Yelishala, K. Kannaiyan, Z. Wang, H. Metghalchi, Y.A. Levendis, R. Sadr, Thermodynamic Study on Blends of Hydrocarbons and Carbon Dioxide as Zeotropic Refrigerants, Journal of Energy Resource Technology, 2020, vol. 142, pp. 082304-082313. doi: 10.1115/1.4045930

[15] G. J. M. Velders, S. O. Andersen, J. S. Daniel, D. W. Fahey, M. McFarland, The importance of the Montreal Protocol in protecting climate, Proceedings of the National Academy of Sciences, 2007, vol. 104, pp. 4814-4819. doi: 10.1073/pnas.0610328104

[16] E. A. Heath, Amendment to the Montreal Protocol on Substances that Deplete the Ozone Layer (Kigali Amendment), International Legal Materials, 2017, vol. 56, pp. 193-205. doi: 10.1017/ilm.2016.2

[17] C. Zhang, C. Liu, X. Xu, Q. Li, S. Wang, Energetic, exergetic, economic and environmental (4E) analysis and multi-factor evaluation method of low GWP fluids in trans-critical organic Rankine cycles, Energy, 2019, vol. 168, pp. 332-345. doi: 10.1016/j.energy.2018.11.104

[18] X. Dai, L. Shi, Q. An, W. Qian, Screening of hydrocarbons as supercritical ORCs working fluids by thermal stability, Energy Conversion and Management, 2016, vol. 126, pp. 632-637. doi: 10.1016/j.enconman.2016.08.024

[19] ANSI/ ASHRAE Standard 34-2016. Retrieved from https://www.ashrae.org/technical-resources/standards-and-guidelines/standards-addenda/addenda-to-standard-34-2016 [accessed on 08.28.2021]

[20] C. Wu, S. Wang, X. Jiang, J. Li, Thermodynamic analysis and performance optimization of transcritical power cycles using CO_2-based binary zeotropic mixtures as

working fluids for geothermal power plants, Applied Thermal Engineering, 2017, vol. 115, pp. 292-304. doi: 10.1016/j.applthermaleng.2016.12.077

[21] G. Shu, Z. Yu, H. Tian, P. Liu, Z. Xu, Potential of the transcritical Rankine cycle using CO_2-based binary zeotropic mixtures for engine's waste heat recovery, Energy Conversion and Management, 2018, vol. 174, pp. 668-685. doi: 10.1016/j.enconman.2018.08.069

[22] J. Mikielewicz, D. Mikielewicz, Comparative study of selected fluids for use in supercritical Organic Rankine Cycles, Archives of Thermodynamics, 2009, vol. 30, pp. 3-14.

[23] R. Vidhi, S. Kuravi, D.Y. Goswami, E. Stefanakos, A.S. Sabau, Organic Fluids in a Supercritical Rankine Cycle for Low Temperature Power Generation, Journal of Energy Resources Technology, 2013, vol. 135. doi: 10.1115/1.4023513

[24] K. Braimakis, M. Preißinger, D. Brüggemann, S. Karellas, K. Panopoulos, Low grade waste heat recovery with subcritical and supercritical Organic Rankine Cycle based on natural refrigerants and their binary mixtures, Energy, 2015, vol. 88, pp. 80-92. doi: 10.1016/j.energy.2015.03.092

[25] M. Chys, M.V.D. Broek, B. Vanslambrouck, M.D. Paepe, Potential of zeotropic mixtures as working fluids in organic Rankine cycles, Energy, 2012, vol. 44, pp. 623-632. doi: 10.1016/j.energy.2012.05.030

[26] J. Radulovic, N.I.B. Castaneda, On the potential of using zeotropic mixtures in supercritical ORC powered by geothermal energy source, Energy Conversion and Management, 2014, vol. 88, pp. 365-371. doi: 10.1016/j.enconman.2014.08.048

[27] B. Saleh, M.S. Youssef, Parametric analysis of an ejector refrigeration cycle activated by renewable energy, International Journal of Mechanical and Production, 2019, vol. 9, pp. 1143-1156. doi: 10.24247/ijmperdjun2019122

[28] Y.A. Cengel, M.A. Boles, M. Kanoglu, Thermodynamics: an engineering approach, vol. 5. New York: McGraw-hill; 2011.

[29] C. Borgnakke, R.E. Sonntag, Fundamentals of thermodynamics. John Wiley & Sons; 2020.

[30] F. Mohammadkhani, N. Shokati, S.M.S Mahmoudi, M. Yari, M.A. Rosen, Exergoeconomic assessment and parametric study of a Gas Turbine-Modular Helium Reactor combined with two Organic Rankine Cycles, Energy, 2014, vol. 65, pp. 533-543. doi: 10.1016/j.energy.2013.11.002

[31] E. Özahi, A. Tozlu, A. Abuşoğlu, Thermoeconomic multi-objective optimization of an organic Rankine cycle (ORC) adapted to an existing solid waste power plant, Energy Conversion and Management, 2018, vol. 168, pp. 308-319. doi: 10.1016/j.enconman.2018.04.103

[32] I. Dincer, M. A. Rosen, Exergy, Exergoeconomic Analysis of Thermal Systems, 2013, Chapter 20, pp. 393-423. Available: 10.1016/C2010-0-68369-6

[33] A. Lazzaretto, G. Tsatsaronis, SPECO: A systematic and general methodology for calculating efficiencies and costs in thermal systems, energy, 2006, vol. 31, pp. 1257-1289.

[34] E. Özahi, A. Tozlu, A. Abuşoğlu, Thermoeconomic multi-objective optimization of an organic Rankine cycle (ORC) adapted to an existing solid waste power plant, Energy

Conversion and Management, 2018, vol. 168, pp. 308-319. doi: 10.1016/j.enconman.2018.04.103

[35] Y. Ceyhun, M. Kanoglu, A. Abuşoğlu, Exergetic cost evaluation of hydrogen production powered by combined flash-binary geothermal power plant, International Journal of Hydrogen Energy, 2015, vol. 40, pp. 14021-14030. doi: 10.1016/j.ijhydene.2015.07.031

[36] X. Zhang, Y. Zhang, Z. Li, J. Wang, Y. Wu, C. Ma, Zeotropic mixture selection for an organic rankine cycle using a single screw expander, Energies, 2020, vol. 13. doi: 10.3390/en13051022

[37] P. Gaspar, P. D. Silva, Handbook of Research on Advances and Applications in Refrigeration Systems and Technologies, Engineering Science Reference, am imprint of IGI Global; 2015.

[38] NOAA Online Weather Data. Retrieved from https://www.weather.gov/wrh/climate?wfo=hgx [accessed on 09.27.2021]